TKK Dissertations 127
Espoo 2008

PHOTOLUMINESCENCE SPECTROSCOPY AND CARRIER DYNAMICS MODELING OF QUANTUM DOT STRUCTURES

Doctoral Dissertation

Hannu Koskenvaara

Helsinki University of Technology
Faculty of Electronics, Communications and Automation
Department of Micro and Nanosciences

TKK Dissertations 127
Espoo 2008

PHOTOLUMINESCENCE SPECTROSCOPY AND CARRIER DYNAMICS MODELING OF QUANTUM DOT STRUCTURES

Doctoral Dissertation

Hannu Koskenvaara

Dissertation for the degree of Doctor of Science in Technology to be presented with due permission of the Faculty of Electronics, Communications and Automation for public examination and debate in Auditorium TU1 at Helsinki University of Technology (Espoo, Finland) on the 13th of June, 2008, at 12 noon.

Helsinki University of Technology
Faculty of Electronics, Communications and Automation
Department of Micro and Nanosciences

Teknillinen korkeakoulu
Elektroniikan, tietoliikenteen ja automaation tiedekunta
Mikro- ja nanotekniikan laitos

Distribution:
Helsinki University of Technology
Faculty of Electronics, Communications and Automation
Department of Micro and Nanosciences
P.O. Box 3500 (Tietotie 3)
FI - 02015 TKK
FINLAND
URL: http://www.micronova.fi/units/mns/
Tel. +358-9-4511
Fax +358-9-451 3128
E-mail: hannu.koskenvaara@tkk.fi

© 2008 Hannu Koskenvaara

ISBN 978-951-22-9413-8
ISBN 978-951-22-9414-5 (PDF)
ISSN 1795-2239
ISSN 1795-4584 (PDF)
URL: http://lib.tkk.fi/Diss/2008/isbn9789512294145/

TKK-DISS-2482

Multiprint Oy
Espoo 2008

ABSTRACT OF DOCTORAL DISSERTATION	HELSINKI UNIVERSITY OF TECHNOLOGY P. O. BOX 1000, FI-02015 TKK http://www.tkk.fi

Author Hannu Koskenvaara

Name of the dissertation

Photoluminescence spectroscopy and carrier dynamics modeling of quantum dot structures

Manuscript submitted June 11, 2007	Manuscript revised
Date of the defence June 13, 2008	
☐ Monograph	☒ Article dissertation (summary + original articles)

Faculty	Faculty of Electronics, Communications and Automation
Department	Department of Micro and Nanosciences
Field of research	Nanotechnology
Opponent(s)	Doc. Antti Kuronen
Supervisor	Doc. Markku Sopanen
Instructor	Doc. Markku Sopanen

Abstract

This thesis deals mainly with the optical investigation of strain induced quantum dots (SIDQ). SIQDs were measured by continuous wave photoluminescence spectroscopy and time resolved photoluminescence, and mathematical models were used to explain the results. Also GaAsN quantum dots on InP, surface passivation of GaAs based structures and indium nitride films were studied.

The SIQDs were formed by manufacturing self assembled nanoscopic islands on top of a quantum well (QW) structure. All the studied materials were III-V compound semiconductors. The influence of the nitrogen concentration on the carrier dynamics in dilute GaInAsN SIQDs was investigated. The small scale lateral variation in the bandgap of the QW is observed. Carrier dynamics was also studied in InGaAsP/InP SIQDs and in coupled GaInAs/GaAs SIQDs. It was found, out, that surface recombination has a more significant role in the InAs islands and wetting layer on top of the InGaAsP/InP structure than in the traditional InP capped GaAs based structures. A rate-equation model was developed to take into account the effect of the surface states by introducing additional terms to the traditional quantum dot recombination and relaxation terms. Modified model agrees well with the measured results. The effect of the gaussian excitation beam distribution was also taken into account in the rate-equation model. The results agree well with the continuous wave PL results from GaInAs/GaAs SIQDs.

Keywords quantum dot, photoluminescence, quantum well, rate-equation

ISBN (printed) 978-951-22-9413-8	ISSN (printed) 1795-2239
ISBN (pdf) 978-951-22-9414-5	ISSN (pdf) 1795-4584
Language english	Number of pages 77 + 66

Publisher Helsinki University of Technology, Department of Micro and Nanosciences

Print distribution Helsinki University of Technology, Department of Micro and Nanosciences

☒ The dissertation can be read at http://lib.tkk.fi/Diss/2008/isbn9789512294145/

VÄITÖSKIRJAN TIIVISTELMÄ	TEKNILLINEN KORKEAKOULU PL 1000, 02015 TKK http://www.tkk.fi
Tekijä Hannu Koskenvaara	
Väitöskirjan nimi Kvanttipisterakenteiden varaustenkuljettajien dynamiikan mallintaminen ja karakterisointi fotoluminesenssimittauksin	
Käsikirjoituksen päivämäärä June 11, 2007	Korjatun käsikirjoituksen päivämäärä
Väitöstilaisuuden ajankohta June 13, 2008	
☐ Monografia	☒ Yhdistelmäväitöskirja (yhteenveto + erillisartikkelit)

Tiedekunta	Elektroniikan, tietoliikenteen ja automaation tiedekunta
Laitos	Mikro- ja nanotekniikan laitos
Tutkimusala	Nanotekniikka
Vastaväittäjä(t)	Dos. Antti Kuronen
Työn valvoja	Dos. Markku Sopanen
Työn ohjaaja	Dos. Markku Sopanen

Tiivistelmä

Työssä tutkittiin pääasiassa jännityksellä aikaansaatujen kvanttipisteiden optisia ominaisuuksia. Kvanttipisteitä tutkittiin fotoluminesenssispektroskopialla ja aikaerotteisin fotoluminesenssimittauksin sekä mallinnettiin matemaattisin menetelmin. Jännitettyjen kvanttipisteiden lisäksi tutkittiin GaAsN-kvanttipisteitä InP-alustakiteellä, GaAs-pohjaisten rakenteiden pintapassivointia ja InN-kerroksia.

Jännitetyt kvanttipisteet valmistettiin kasvattamalla itseorganisoituvia nanoskooppisia saarekkeita kvanttikaivorakenteen pinnalle. Työssä käytettiin materiaaleina III-V -yhdistepuolijohteita. Tutkittaessa typpikonsentraation vaikutusta varauksenkuljettajien dynamiikkaan GaInAsN-kvanttipisterakenteissa havaittiin kvanttikaivon energia-aukon arvon lyhyen kantaman variaatiota. InGaAsP/InP-kvanttipisteitä tutkimalla havaittiin, että pintarekombinaatiolla on paljon suurempi merkitys InAs-saarekkeissa ja -kastumiskerroksessa InP-pohjaisen rakenteen päällä kuin InP-saarekkeissa ja -kastumiskerroksessa GaAs-pohjaisen rakenteen päällä. Kvanttipisteiden varauksenkuljettajien dynamiikan mallintamisessa käytettyä taseyhtälömallia kehitettiin lisäämällä malliin pintatilojen ja kvanttirakenteiden elektronitilojen välisiä siirtymiä mallintavat termit. Paranneltu malli ennustaa hyvin InGaAsP/InP-kvanttipisteistä tehdyt kokeelliset havainnot. Taseyhtälömallia kehitettiin myös jatkuvaviritteisen fotoluminesenssin mallintamiseen sopivaksi huomioimalla virityssäteen intensiteetin gaussinen jakauma. Kehitetty malli ennustaa GaInAs/GaAs-kvanttipisterakenteesta mitatut tulokset hyvällä tarkkuudella.

Asiasanat kvanttipiste, fotoluminesenssi, kvanttikaivo, taseyhtälö	
ISBN (painettu) 978-951-22-9413-8	ISSN (painettu) 1795-2239
ISBN (pdf) 978-951-22-9414-5	ISSN (pdf) 1795-4584
Kieli englanti	Sivumäärä 77 + 66
Julkaisija Teknillinen korkeakoulu, Mikro- ja nanotekniikan laitos	
Painetun väitöskirjan jakelu Teknillinen korkeakoulu, Mikro- ja nanotekniikan laitos	
☒ Luettavissa verkossa osoitteessa http://lib.tkk.fi/Diss/2008/isbn9789512294145/	

Preface

The work for this thesis has been carried out at Optoelectronics Laboratory of Helsinki University of Technology during 1999–2006. I want to express my gratitude to Docent Markku Sopanen, the supervisor of this thesis, for his continuous support and advice with the manuscripts. I would like to express my gratitude to Prof. Turkka Tuomi, who was my supervisor before he retired. I thank Prof. Harri Lipsanen and prof. Turkka Tuomi for the opportunity to work in the laboratory. The financial support of the Graduate School of Electronics, Telecommunications and Automation is gratefully acknowledged.

I want to thank my co-workers. I had fruitful co-operation with Teppo Hakkarainen, Juha Toivonen and Päivi Pohjola in the work involving dilute nitrides and with Juha Riikonen, Jaakko Sormunen, and Marco Mattila with the InGaAsP/InP-structures. Marco Mattila has also fabricated samples used in my coupled quantum dot work. I thank also Sami Suihkonen and Victor-Tapio Rangel-Kuoppa for co-operation in indium nitride research. I want to thank all the personnel in our laboratory for the excellent working atmosphere.

I want to thank my parents Pirjo and Heikki for their support to my lifelong interest to empirical research. Last but not least, I want to thank my wife Anneli and my twin daughters Eija and Essi for bringing delighful content into my life during the years worked with this thesis.

Contents

Preface **vii**

Contents **ix**

List of Publications **xi**

Author's contribution **xiii**

1 Introduction **1**

2 Semiconductor quantum structures **3**

2.1 Basic semiconductor properties 3

2.2 Quantum structures 6

2.3 Fabrication of quantum structures 6

3 Strain induced quantum dots **10**

3.1 Structure 10

3.2 Modeling of electronic states 11

3.3 Carrier dynamics 17

4 Characterization methods **20**

4.1 Continuous wave photoluminescence spectroscopy 20

4.2 Time resolved photoluminescence 22

4.3 Atomic force microscopy 23

5 SIQD results **26**

5.1 SIQDs with dilute nitrides 26

5.2 Carrier dynamics in InGaAsP/InP SIQDs 30

5.3 Surface effects in InGaAsP/InP SIQD structure 33

5.4 Effect of gaussian beam distribution in rate equation model 39

5.5 Modeling and PL study of coupled QDs 42

6 Other results **45**

6.1 GaNAs QDs on InP 45

6.2 GaN passivation of GaAs surface QW 49

6.3 Optical properties of InN 52

7 Summary **55**

References **57**

List of Publications

This thesis consists of an overview and of the following publications which are referred to in the text by their Roman numerals.

I H. Koskenvaara, T. Hakkarainen, M. Sopanen, and H. Lipsanen, *Photoluminescence study of strain-induced GaInNAs/GaAs quantum dots*, Journal of Materials Science: Materials in Electronics **14**, 357–360 (2003).

II J. Riikonen, J. Sormunen, H. Koskenvaara,M. Mattila, M. Sopanen, and H. Lipsanen, *Highly Tunable Emission from Strain-Induced InGaAsP/InP Quantum Dots*, Japanese Journal of Applied Physics **44**, L976 (2005).

III H. Koskenvaara, J. Riikonen, J. Sormunen, M. Sopanen, and H. Lipsanen, *Carrier dynamics in strain-induced InGaAsP/InP quantum dots*, Physica E **32**, 179–182 (2006).

IV J. Riikonen, J. Sormunen, H. Koskenvaara, M. Mattila, A. Aierken, T. Hakkarainen, M. Sopanen, and H. Lipsanen, *Effect of surface states on carrier dynamics in InGaAsP/InP stressor quantum dots*, Nanotechnology **17**, 2181–2186 (2006).

V Hannu Koskenvaara, Marco Mattila, Markku Sopanen, and Harri Lipsanen, *Carrier Dynamics in Strain Induced Quantum Dots Modeled by Rate Equations and Gaussian Excitation Beam Distribution*, Japanese Journal of Applied Physics **47**, 5499–5502 (2008).

VI P. Pohjola, T. Hakkarainen, H. Koskenvaara, M. Sopanen, H. Lipsanen, and J. Sainio, *Tensile-strained GaAsN quantum dots on InP*, Applied Physics Letters **90**, 172110 (2007).

VII J. Riikonen, J. Sormunen, H. Koskenvaara, M. Mattila, M. Sopanen, and H. Lipsanen, *Passivation of GaAs surface by ultrathin epitaxial GaN layer*, Journal of Crystal Growth **272**, 621–626 (2004).

VIII S. Suihkonen, J. Sormunen, V.T. Rangel-Kuoppa, H. Koskenvaara, and M. Sopanen, *Growth of InN by vertical flow MOVPE*, Journal of Crystal Growth **291**, 8–11 (2006).

Author's contribution

The author has written the manuscripts for publications I, III, and V. The author has planned and carried out continuous wave PL measurements for publications I, III, IV (partly), V, VII and VIII and time resolved PL measurements for publications I, III, IV, V. Atomic force microscope studies for publication I were also performed by the author.

The author has made the rate-equation modeling for publications II, III, IV, and V. Author has also calculated the electronic states of the quantum well for publication VII.

The author has also participated in the discussions concerning optical spectroscopy, modeling and interpretation of results for publications II, IV, VI, VII and VIII.

1 Introduction

The first semiconductor was discovered in 1833, when Michael Faraday discovered that the resistivity of silver sulfide decreases as the temperature is increased. However, it took about a century before knowledge in the physics of semiconductors was grown to the level that the first applications were developed. Invention of the transistor in 1948 was a major breakthrough for semiconductors. After that a huge amount of applications in nearly all the sectors of everyday life have given to the semiconductor technology a major role in the global industry and research facilities. Research and fundamental understanding of semiconductors have developed hand in hand with the applications.

Undoubtfully the most important semiconductor is silicon. It is the basic material of electronics. Also light emission from silicon is intensively studied, because that would make it possible to combine electronic and optical functions in the same integrated circuit at low costs. However, the success has been unsatisfactory, because silicon has an indirect bandgap, which is a fundamental problem for emission of light. The major materials in optoelectronics are the III–V compound semiconductors. Maybe the most important application of optoelectronics is the optical telecommunication, which constitutes a significant part of the global telecommunication system.

Developments in manufacturing have made it possible to approach fundamental limits of materials. When the size of structures is miniatyrized to the nanometer scale, quantum mechanical effects begin to rule physical phenomena. In the last decade, a new field of technology called nanotechnology has been distinguished because the feature sizes of the structures are in the nanometer scale. A major part of this thesis concentrates on quantum structures, which can be included into the field of nanotechnology. Properties of quantum wells and quantum dots are inves-

tigated mainly by photoluminescence (PL) spectroscopy. Theoretical work is made to develop mathematical models to predict the observed optical behaviour.

In publication I electronic states and carrier dynamics of the novel GaInNAs strain induced quantum dot (SIQD) structure are studied with continuous wave and time resolved photoluminescence for the first time. In publication II a novel GaInAsP/InP SIQD material system is studied by photoluminescence and theoretical models. In publications III and IV the effect of surface states in GaInAsP/InP SIQDs is investigated. In publication V continuous wave PL is modeled with rate equations taking into account gaussian excitation beam distribution. In publication VI tensile strained GaAsN quantum dots (QDs) on InP are studied. The PL measurements suggest that there may be type-I junction between GaAsN dots and InP, which enhances possibilities to utilize this material system in optical devices. In publication VII *in situ* surface passivation of GaAs was investigated. It is observed, that a thin GaN layer protects the GaAs surface from ambient air and reduces the surface recombination rate. In publication VIII one of the least known of III–V semiconductors, InN, was fabricated and investigated by different methods.

A short introduction to semiconductors related to this thesis, quantum structures, and their fabrication is given in chapter 2. Chapter 3 describes the physical properties of the SIQD structure and the modeling methods used in this thesis. The experimental methods are discussed in chapter 4. Chapter 5 presents results related to SIQDs and chapter 6 describes other results. The main results of this thesis are summarized in chapter 7.

2 Semiconductor quantum structures

This chapter gives a brief introduction to quantum dots ond other quantum structures used in this thesis. The basic properties of semiconductors and the materials used in this thesis are shortly introduced in section 2.1. In section 2.2 the quantum structures with different dimensionality are presented. Section 2.3 describes some fabrication methods of semiconductor quantum structures.

2.1 Basic semiconductor properties

Semiconductors are materials, which have a moderately low band gap energy. Doping of semiconductor with controlled amounts of impurities makes it possible to generate electrons in the conduction band or empty states, so called holes, in the valence band. This makes it possible to control the electric properties of the semiconductor, because the electrons and the holes can act as charge carriers. The carriers can also be generated by exiting the electrons from the valence band to the conduction band with light, and in certain semiconductors, which have a direct bandgap, recombination of carriers can also produce light with good efficiency. Therefore, semiconductors can be used to convert electric signals to optical and *vice versa*.

With modern epitaxial fabrication methods semiconductor materials can be combined to form heterojunctions, that are nearly perfect. The two most common heterojunction types are shown in figure 2.1. Typically type-I junctions are favored in quantum structures made for optical purposes. In type-I junction both carriers are confined in the same area in the semiconductor crystal, whereas in type-II junction electrons and holes are localized in different regions. In the type-I quantum structure the wavefunctions of the electrons and holes have larger overlap, and, therefore, the probability of the optical transitions is higher.

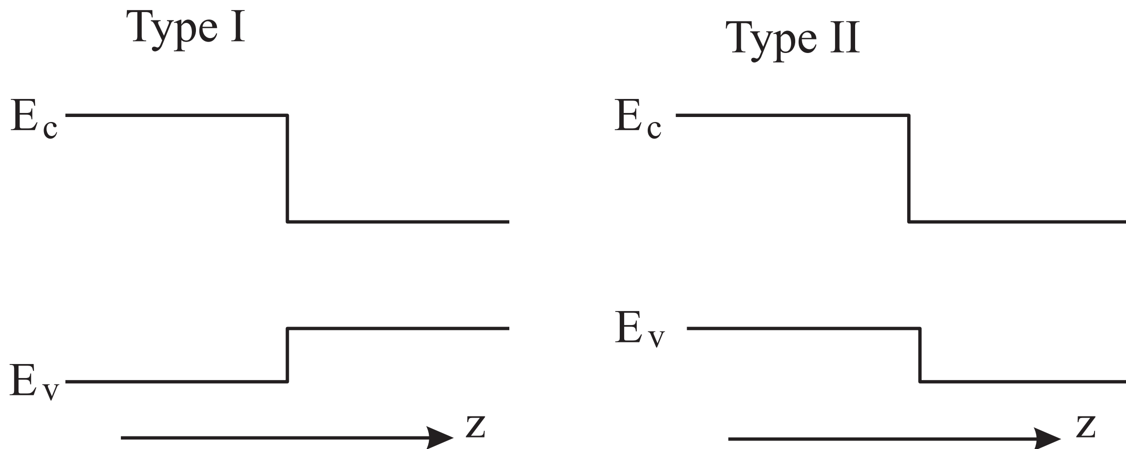

Figure 2.1: Different types of semiconductor heterojunctions. E_c and E_v are the energies of the conduction and valence band edges.

Binary compounds have a fixed lattice constant and a bandgap energy, which severely restricts possibility to engineer the structures to have predetermined properties, for example to choose the wavelength in a light emitting diode. Ternary or quaternary alloys give more controllability to the properties of the semiconductor structures. For a ternary compound, *e.g.*, $In_xGa_{1-x}As$, either the bandgap or the lattice constant can be selected by setting the value of x. The quaternary compounds, *e.g.*, $In_xGa_{1-x}N_yAs_{1-y}$, have two composition parameters, x and y, which make it possible to control both the lattice constant and the bandgap. This is essential, if, for example, a thick layer of semiconductor with determined bandgap is fabricated on top of a GaAs substrate, which fixes the lattice constant.

In this work, several binary compounds and ternary and quaternary alloys are used. $In_xGa_{1-x}As$ and $In_xGa_{1-x}N_yAs_{1-y}$ were fabricated on GaAs substrates to make QWs. By increasing the indium concentration x, the bandgap can be lowered from the GaAs value of 1.519 eV towards the values of 0.95 or 0.8 eV, which are the most usable photon energies in telecommunication applications. However, if $In_xGa_{1-x}As$ is grown on GaAs, the strain increases with the increasing In consentration. If the

In concentration is increased sufficiently to achieve the telecommunication energy range, the strain induced dislocations are too numerous for a satisfactory component action. This energy range can be reached by using InP, which has larger lattice constant than GaAs, as a substrate, but unfortunately InP laser structures have some shortcomings such as low characteristic temperature and difficulties in fabrication of Bragg mirrors for vertical cavity surface emitting lasers (VCSELs). On the other hand, $In_xGa_{1-x}As$ at low indium concentrations ($x \approx 0.1$) is an excellent material to produce high quality quantum structures for scientific purposes.

The bandgaps of GaAs and InGaAs decrease dramatically, if a small part of As atoms is replaced with N atoms. Typically the nitrogen consentration is 0–6 %, and the telecommunication wavelengths can be achieved at under 5 %. In the recent decade, these so called dilute nitrides GaN_yAs_{1-y} [1] and $In_xGa_{1-x}N_yAs_{1-y}$ [2] grown on GaAs substrates have been intensively studied. $In_xGa_{1-x}N_yAs_{1-y}$ was first proposed by Kondow *et al.* [2]. This material can be lattice matched to the GaAs substrate and have the bandgap in the telecommunication region.

Also $In_xGa_{1-x}As_yP_{1-y}$ grown on InP substrates was used in this work. $In_xGa_{1-x}As_yP_{1-y}$ is a highly tunable material which is used for QW and SIQD structures. It can simultaneously be lattice matched to the InP substrate and produce the bandgap in the telecommunication wavelengths.

Also the binary compound InN was fabricated on sapphire substrate in this thesis. InN has not been studied very intensively. Properties of InN are relatively poorly known, even its bandgap is somewhat uncertain. Many previous studies have reported values near 2 eV [3] but new measurements of high quality InN films have shown evidence of a much smaller band gap between 0.65 and 0.90 eV [4]. This value is compatible with the main wavelength range of the optical telecommunication and suggests that InN may be useful in some applications. Additionally, InN has excellent electron transport properties predicted theoretically [5].

2.2 Quantum structures

Quantum structures are structures, in which quantum mechanical effects arising from the structure itself have significant influence on the behaviour of the carriers. For typical III–V semiconductors quantum mechanical effects arise, when the dimension is in the order of 10 nm [6]. The properties of the quantum structure depend on how many dimensions the carriers are confined in. In a quantum well (QW) the carriers are confined in one dimension. They can move laterally in the QW, but not in perpendicular direction. This causes energy quantization in the direction perpendicular to the QW layer. In a quantum wire the carriers are confined in two dimensions and can move only in one dimension. Finally, in a quantum dot (QD) the movement of the carriers is restricted in all three dimensions. These quantum structures and their density of states for electrons are shown schematically in figure 2.2. The density of states shows more concentration near the quantized energy levels, when the dimensionality of the quantum structure is reduced. In QDs the carriers only have discrete energy states like in an atom. However, quantum numbers defining a certain state are different than in an atom due to the different geometry of the confinement potential.

The quantum structures have applications in electronics, especially in optoelectronic devices. Quantum structures can be used, for example, to achieve population inversion in the active QW layer of the semiconductor laser at lower current density then in a bulk material.

2.3 Fabrication of quantum structures

Typically semiconductor QWs are fabricated by epitaxially growing a thin layer of low bandgap material between barrier layers of a larger bandgap material. Mod-

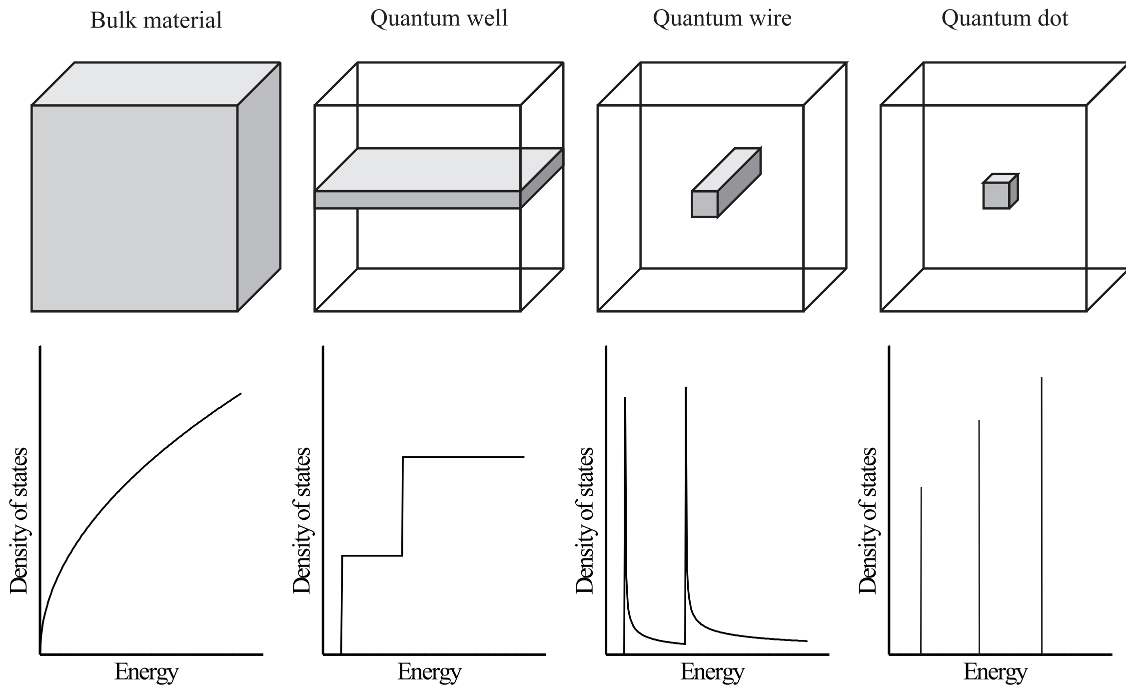

Figure 2.2: Schematic structure and density of states function for electrons in a bulk semiconductors and different quantum structures.

ern epitaxial fabrication methods, for example, metal organic vapor phase epitaxy (MOVPE) or molecular beam epitaxy (MBE), can make very sharp interfaces between the layers. The samples used in this work were fabricated by MOVPE. Trimethylgallium, trimethylindium, tertiarybutylphosphine, tertiarybutylarsine and dimethylhydrazine were used as percursors for gallium, indium, phosphorus, arsenic and nitrogen, respectively. The precursors were transported from bubblers to the reactor by using hydrogen as a carrier gas. The flow rate of the precursors was controlled by mass flow controllers. In the reactor the precurcors dissociate at a high temperature and most of the metal atoms and the group V atoms are adsorbed to the surface. The particles can migrate on the surface and they have a tendency to migrate to an energetically favorable position on the edge of the monolayer step or to form clusters with the other particles. Particles can also desorb from the surface. The rates of these processes are affected by growth parameters, such as temperature

or partial pressures of the constituents [7]. Growth temperatures used in this work were between 550 °C and 650 °C. The MOVPE reactor was also used for *in situ* annealing of some of the samples in this thesis.

There are many methods to fabricate III–V semiconductor QDs. The methods can be divided into two classes. In top-down methods the QDs are fabricated by removing material, for example by selective etching using nanospheres as an etching mask [8]. In bottom-up methods the QDs are formed by selectively growing material on the surface, *e.g.*, by the self assembled island growth.

There are three different growth modes in heteroepitaxy. These are shown in figure 2.3. In Frank–van der Merwe mode the crystal grows layer by layer [9] and in the Volmer–Weber mode the islands grow directly on the surface without the wetting layer [10]. In Stranski–Krastanow (S–K) mode [11] the growth starts with the layer by layer growth mode. However, the epitaxial layer is strained due to the difference in the lattice constants. The strain energy increases when the layer thickness increases, and after the critical thickness is reached, it is energetically more favorable to form islands, in which strain is relaxed by dislocations, than to continue layer by layer growth mode. Typically the critical thickness is a few monolayers in III–V quantum structures consisting of materials having a lattice constant difference of a few percent. The thin planar layer is called a wetting layer.

Dislocations, which are formed in the island, are very detrimental to the performance of optoelectronic components. However, in 1990 Eaglesham and Cerullo reported that Ge islands on Si do not have dislocations. This growth mode is now called coherent S–K mode. The coherent S–K mode has been observed in growth of many III–V material systems, *e.g.*, InGaAs/GaAs [13], InAs/GaAs [14], InGaAs/AlGaAs [15], InP/GaAs [16], InAs/InP [17], and GaSb/GaAs [18], and it is the most important method for fabrication of self assembled III–V QDs.

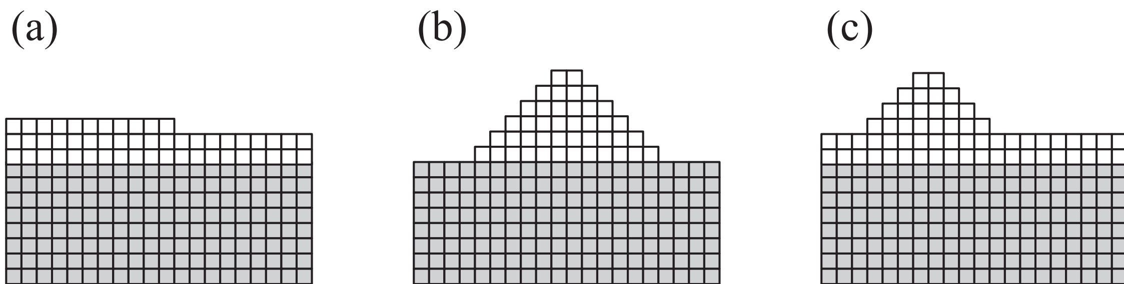

Figure 2.3: Heteroepitaxial growth modes. (a) Frank–van der Merwe mode, (b) Volmer–Weber mode, and (c) Stranski–Krastanow mode.

3 Strain induced quantum dots

An introduction to strain induced quantum dot (SIQD) sturctures investigated in this thesis is given in this chapter. Section 3.1 describes the structure of the SIQDs. In section 3.2 the electronic states and their calculation in SIQDs are discussed. Section 3.3 introduces carrier transition processes that are the most significant for interpreting optical measurements and discusses the models which are used to simulate carrier dynamics in SIQDs.

3.1 Structure

Strain induced quantum dots (SIQD) have been investigated for about two decades. Kash *et al.* reported QDs induced by lithographically patterned stressors from strained semiconductor layer in 1988 [19]. The first self assembled SIQDs were reported by Sopanen *et al.* in 1994 [16]. SIQDs can also be fabricated by using buried stressors under the QW [20], and by using non-semiconducting stressor materials, *e.g.*, carbon [21] or tungsten [22].

In SIQD structures used in this thesis coherent self assembled islands are fabricated on top of a standard near surface QW structure. An atomic force microscope image of the islands is shown in figure 3.1 (a). The lattice constant of the island material is larger than the lattice constant of the substrate. Therefore, the island induces a tensile strain in the substrate. The QW layer is pseudomorphic, *i.e.*, the lateral lattice constant of the QW is the same as the lattice constant of the substrate. Therefore, the QW layer is compressively strained. However, the strain induced by the stressor island to the QW structure is tensile under the stressor. The scematic picture of SIQD structure and approximated hydrostatic strain field in a typical SIQD structure are shown in figure 3.1 (b) and (c), respectively. The strain field in

the structure modulates the band edges to form a lateral potential well for both the electrons and the holes. This potential os shown in figure 3.1 (d). Together with the vertical confinement potential of the QW, the lateral confinement potential forms a QD in the QW layer. The lateral potential of the QD is nearly parabolic, especially near the center in the conduction band.

3.2 Modeling of electronic states

The strain field in the structure under the stressor is calculated with the commercial FEM-modeling program Ansys [23]. The geometry of the structure is assumed to be cylindrically symmetric, which reduces the computationally demanding three dimensional problem into two dimensions. The material parameters are taken from ref. 24. The calculations are made for single and double QD structures. However, the best fitting to measurements was obtained when the strain potentials are calculated without the QW layer (*i.e.*, having only the substrate under the island) and the QW potential determined from the experimental PL measurements is then added to the strain potential. This is quite logical since possible variations in fabrication parameters make it difficult to determine the exact composition of the QW. The band offset of the conduction band is 77 % of the whole bandgap energy difference in the GaAs/$In_{0.1}Ga_{0.9}As$ QW [25]. The calculated hydrostatic strain is shown in figure 3.1 (c).

The strain in a crystal modifies the electron bands so, that the potential minimas for the electrons and holes are formed in the tensilely strained area under the stressor. The effect of the strain to the band edges can be taken into account by $\mathbf{k} \cdot \mathbf{p}$ theory [26, 27]. The shift in the energy of the conduction band can be written as

$$V_c = a_c(\epsilon_{xx} + \epsilon_{yy} + \epsilon_{zz}). \tag{3.1}$$

The deformation potential of the conduction band a_c is the material parameter. The

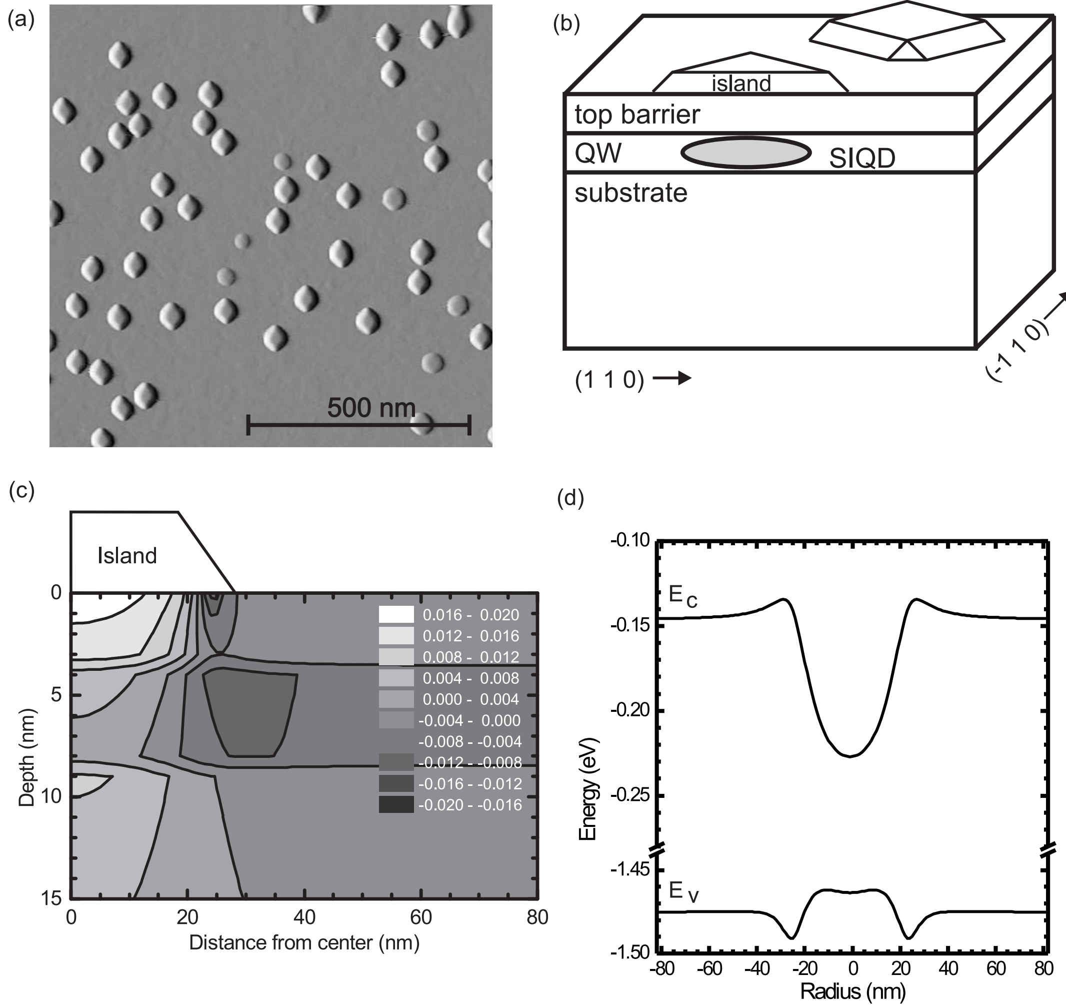

Figure 3.1: (a) Atomic force microscope image from the surface of the sample. Stressor islands with the diameter of 70 nm, the height of 15 nm, and shape typical for the compressively strained stressors studied in this thesis can be clearly seen. (b) Schematic illustration of a strain induced quantum dot structure. The quantum dot is in the quantum well, not in the island on the surface. (c) Hydrostatic strain in a SIQD structure. The horizontal compressively strained (negative values) layer with abrupt edges is the QW. The SIQD is formed in the tensilely strained area under the stressor. The strain field inside the stressor island is not shown in the figure. Notice the different length scales of the axes. (d) Band edges in the QW under the stressor island. Energy values are compared to the conduction band edge of unstrained substrate material.

lateral potential is near parabolic, especially near the center of the SIQD, which lead to degeneration and even spacing of energy states [28].

The influence of the strain to the valence band is more complicated. In this work the simplified two band model is used. The strain splits the degeneracy of heavy hole and light hole bands at Γ-point. In a tensilely strained material the energy of the light hole band edge is few tens of meV lower than the energy of the heavy hole band edge. Thus, the coupling between the hole bands is neglected and only the heavy holes are taken into account. More detailed presentation of the approximations used can be found in ref. 29. Tulkki and Heinämäki [29] report also, that their model agrees well with the experimental results of Lipsanen *et al.* [30]. The strain potential of the heavy hole band is

$$V_v = a_v(\epsilon_{xx} + \epsilon_{yy} + \epsilon_{zz}) - b_v(\epsilon_{zz} - 1/2(\epsilon_{xx} + \epsilon_{yy})). \tag{3.2}$$

The deformation potentials of valence band, a_v and b_v, depend also on the material. The values for GaAs and InAs used in this work are taken from ref. 24, and the deformation potentials of InGaAs are approximated linearly from the values of GaAs and InAs. The calculated valence and conduction band edges in the double QD structure are shown in figure 3.2.

The QD states can be labeled by the radial quantum number n and the angular momentum quantum number $m = 0, \pm 1, \pm 2, \ldots$. These states are denoted as $n\Sigma$, $n\Pi$, $n\Delta$, $n\Phi$,..., in which Σ, Π, Δ, and Φ correspond to the m values of 0,±1,±2,±3, respectively. The lowest state, corresponding to the PL peak QD0 is 1Σ. The next in the energy scale are the degenerate states $1\Pi^{\pm}$, in which ± corresponds to the positive and negative values of m (PL peak QD1). The next higher states are 2Σ and $1\Delta^{\pm}$, which are nearly degenerate .The energy difference between them is only about 1 meV, which can not be resolved from the QD2 peak in the PL measurements due to the linewidth of the QD peaks. The next state set is the nearly degenerate $2\Pi^{\pm}$ and $1\Phi^{\pm}$ (QD3). The degeneracy would be perfect and the energy differences of

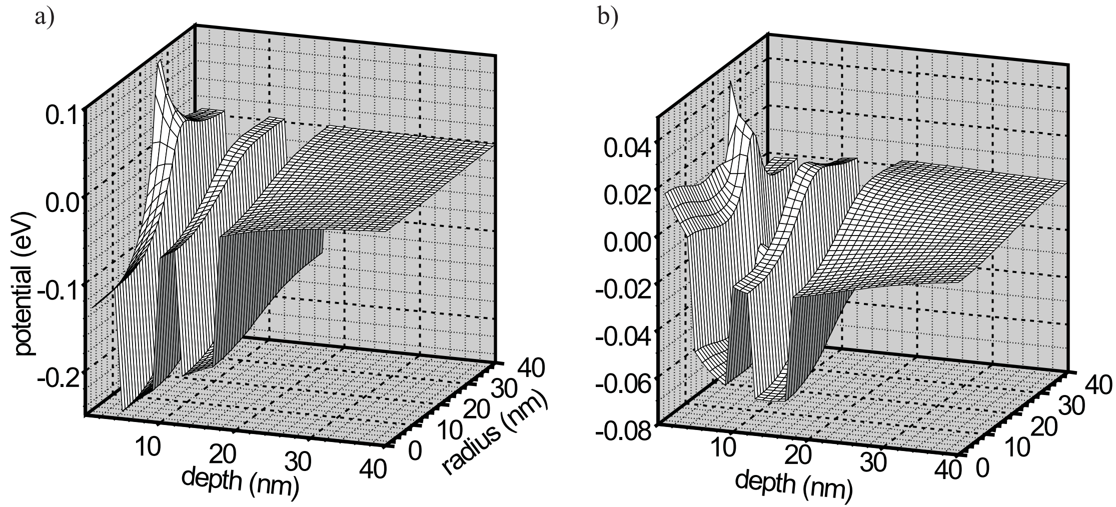

Figure 3.2: Confinement potentials of the (a) conduction and (b) valence bands under the stressor in the double QD structure. The geometry is cylindrical symmetric. The radius is measured from the symmetry axis and the depth is measured from the surface of the top barrier. The zero level of the potential is the band edge of GaAs without any stressor induced strain.

consecutive states would be constant, if the lateral potential were exactly parabolic.

In the past few years, coupled QDs have been fabricated by growing several layers of self assembled islands separated by a layer of the barrier material [31, 32]. Coupled SIQDs have also been fabricated by modulating the band gap of near surface quantum wells [33, 34]. In the coupled QDs there are two potential minima under the stressor. A barrier between the minima is so thin, that overlapping of the wavefunctions affects significantly the electronic states of the system. Symmetric electron states, in which the wavefunction has the same sign on both minimas, are much like the electron states in a single QD. In addition to the symmetric states, also the corresponding set of antisymmetric electron states may exist in double QDs. Their energies are larger than those of the symmetric states. Ren *et al.* have observed these states in PL spectra [34]. Some calculated wave functions of the double QD are shown in figure 3.3.

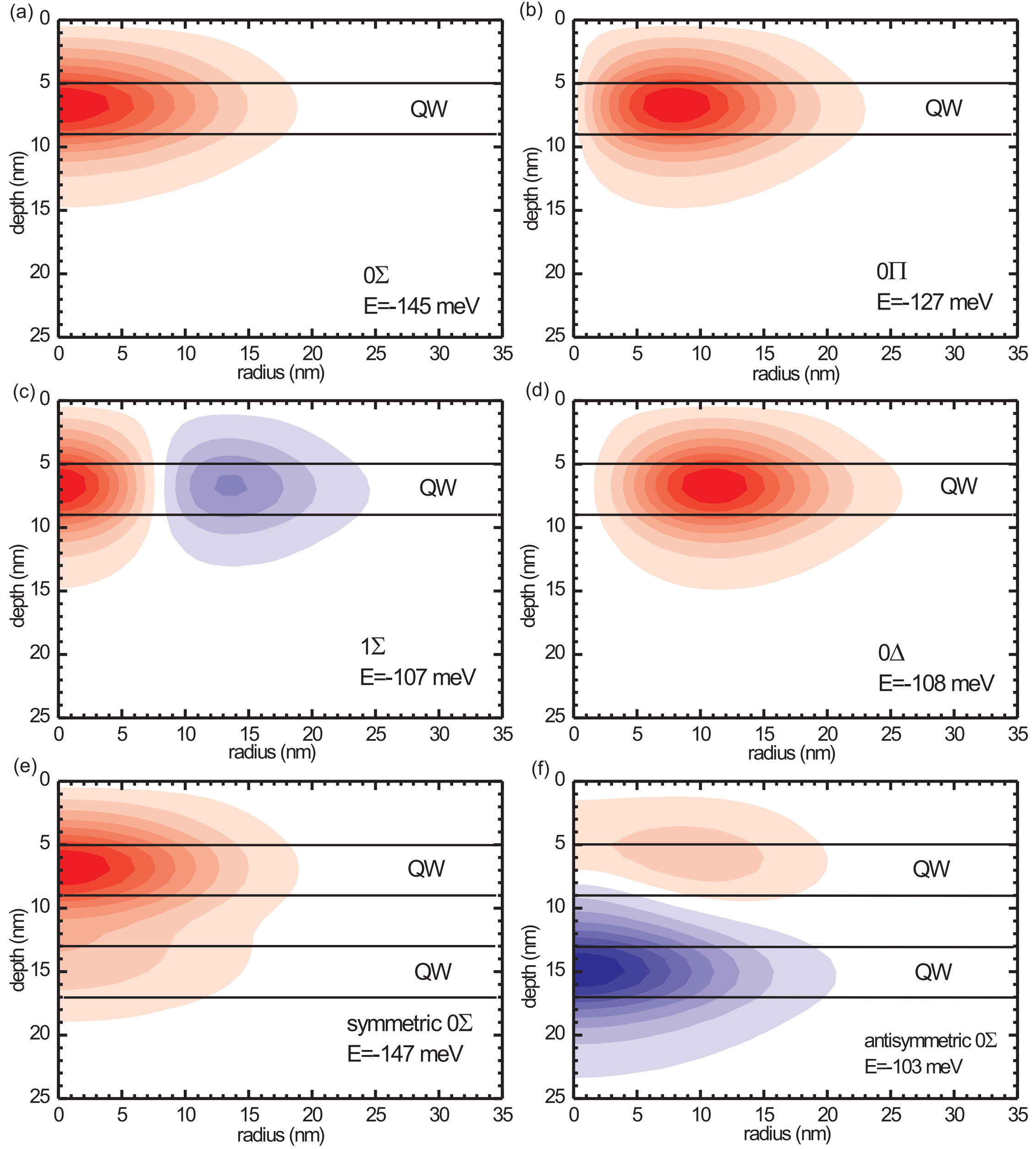

Figure 3.3: Electron wave functions of different QD states: (a)-(d) single QD states, (e) symmetric ground state, and (f) the lowest antisymmetric state in a coupled SIQD. Depth is measured from the upper surface of the top barrier (the stressor is not shown in the graphs) and radius is the distance from the center of the cylindrical symmetry axis (*i.e.*, the center of the island).

Actually, the shape of the island is a truncated hexagonal pyramid, shown in figure 3.1. The long side of the island base is oriented along [1 1 0] direction. Virkkala *et al.* have calculated SIQD potentials with a 3D model and discussed their effects on carrier dynamics [35]. In 3D the shear strain terms cause a significant piezoelectric effect on the band edges. For electrons two potential minima, of which the depths are comparable to the main minima induced by the hydrostatic deformation, form few tens of nanometers to [1 1 0] and [-1 -1 0] directions from the center. For holes, minimas appear in [1 -1 0] and [-1 1 0] directions. For the few first carriers it is energetically more favorable to go into the piezominima than into the deformation minima. However, due to the spatial separation of different carriers, the lifetime of these carriers is very long. Also the radiative lifetimes between the carriers in the piezominima and the defromation minima are approximately three orders of magnitude larger than the radiative lifetimes of the carriers in the deformation minima. Therefore, under photoexcitation the carriers trapped into the piezominima screen the piezopotential and have minor influence on the PL of the QDs, although the depths of these potential minima are very signigicant compared to the deformation minimum. However, the trapped carriers in the piezominima can have a major role in the relaxation processes in the QD.

The model used in this work also ignores many particle interactions. Due to these interactions, the energy states of the QD change, when the population in the QD changes. This effect can not be detected in normal PL measurements, because the inhomogenous broadening of the spectral lines is too large. However, theoretically predicted Coulomb correlations have been observed in a micro-PL experiment conducted to a single QD on a mesa-like structure [36].

3.3 Carrier dynamics

The transitions of the carriers between the energy states in a SIQD structure can be divided into recombination and relaxation. Recombination is a transition, in which the electron in conduction band and the hole in valence band annihilate and release their energy as a photon or phonons. The most significant recombination processes in SIQD samples are radiative recombination in the QD, the QW and the bulk substrate. It has been shown that recombination in the QD mainly obeys the selection rules $l_{\text{initial}} = l_{\text{final}}$ and $n_{\text{initial}} = n_{\text{final}}$. However, especially at higher states, where the lateral potential is farther from the ideal parabolic form, recombination between different n states can also occur [29]. The recombination processes and the corresponding peaks in the PL spectrum are shown in figure 3.4. Also surface recombination plays a major role in the carrier dynamics in InP-based SIQDs [Publication III]. In GaAs-based SIQDs, the InP wetting layer and the InP islands passivate the surface so that the surface processes do not have a very significant effect [37].

The intraband transitions are called relaxation process. The most important relaxation processes in SIQDs are shown in figure 3.5. In time resolved PL measurements, the carriers are generated with an intense 150 fs excitation pulse. The pulse generates carriers mainly in the bulk of semiconductor, because the quantum structures are too thin to absorb significant amount of light. The carriers are rapidly thermalized near to the band edges and subsequently to the QW and QD states. This process is mediated by the Coulomb scattering and the longitudinal optical (LO) phonon emission. At high QW carrier density, Coulomb scattering in the QW is the most prominent relaxation process from the QW to the QDs [38]. The risetime of the luminecsence of the QD ground state has been measured to be 0.45 ps after the excitation pulse at the excitation density of $2.3 \cdot 10^{17}\text{cm}^{-3}$ [39]. At lower carrier densities the Auger and LO phonon relaxation processes dominate the relaxation from QW to QD [40]. In the Auger process the relaxing electron donates its energy and momentum to the hole, which is excited from the QD to the QW. Typically the

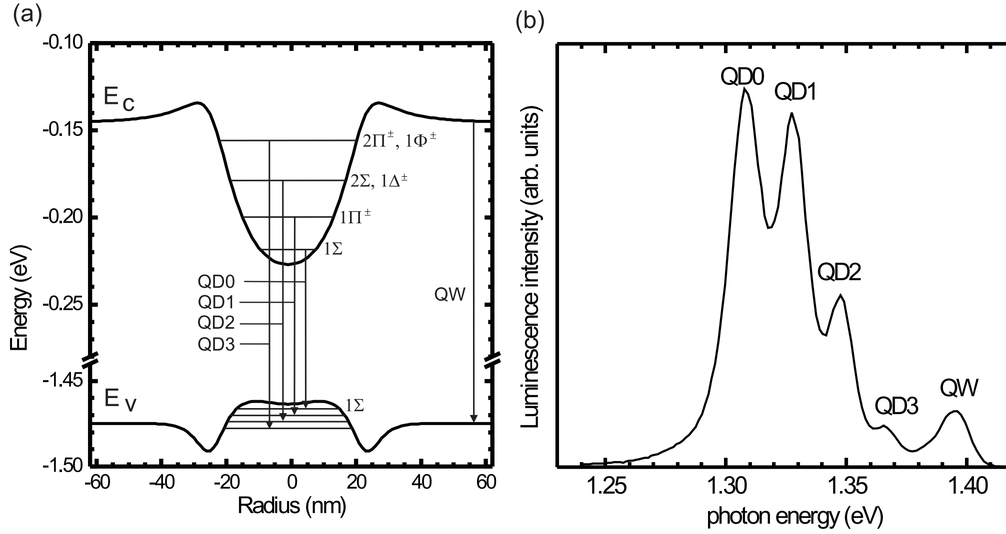

Figure 3.4: (a) Band edges of a SIQD. The potential in the conduction band is nearly parabolic. Recombination between the QD states is denoted by QD0–QD3 and recombination in the QW is noted as QW. (b) A PL spectrum of a SIQD sample. PL peaks corresponding to transitions QD0–QD3 and QW are labeled in the figure.

Auger process is the most important relaxation process between the QD states [41], but in the special QDs with the electron state spacing near the LO phonon energy LO phonon relaxation can be very effective [42]. In the valence band, in which the spacing of the energy levels is small, the longitudinal acoustic (LA) phonon scattering is an effective mechanism.

There are two main methods to model the carrier dynamics: rate-equations and master equations. In this work the rate-equation model is used. The detailed description of the basic rate equation model is given by Grosse *et al.* [43]. In the rate equation model populations of the QD states are averaged over the ensemble of QDs. In this thesis the rate equation model is expanded to explain transitions to the surface states in InGaAsP/InP SIDQs [publications III and IV] and measured continuous wave PL intensities of the QD states [publication V]. Detailed discussion of the modifications can be found in chapters 5.3 and 5.4, respectively.

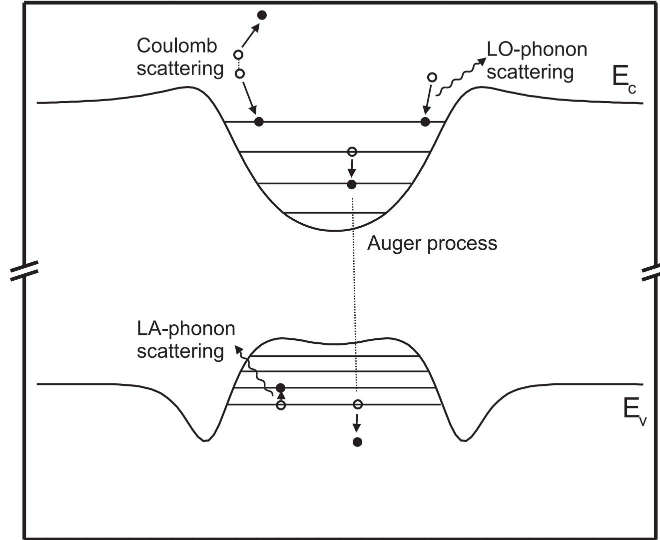

Figure 3.5: Some relaxation processes which affect the carrier dynamics in a SIQD. The processes are explained in more detail in the text.

The more detailed master equation model takes into account the separate microstates [44]. However, there is a problem of defining the initial state populations of the microstates, which can not be uniquely determined from the measured PL data. The master equation model is also computationally very demanding. Therefore, the more simple rate equation model is often used instead of the master equations. Grundmann *et al.* [45] have compared these two models with the same PL data. Master equations agree well with the measured results, but the difference to the predictions of the rate equation model is relatively small, if the relaxation time constant is not significantly smaller than recombination time constant. In the SIQDs investigated in this thesis the predictions of the rate-equation model are, therefore, sufficiently accurate at low carrier densities. At high carrier densities (shortly after the excitation pulse) the intensive Coulomb scattering reduces the relaxation time constant and the rate equation model does not describe the carrier dynamics adequately.

4 Characterization methods

The characterization methods used in this work are introduced in this chapter. The continuous wave and the time resolved photoluminescence measurement systems are described in sections 4.1 and 4.2, respectively. Section 4.3 discusses the atomic force microscopy (AFM) used to characterize the surfaces of the samples.

4.1 Continuous wave photoluminescence spectroscopy

The electronic structure of the sample can be characterized with the photoluminescence (PL) method. In a PL measurement, electron-hole pairs are generated by photons of light. Typically, the excitation photon energy is in the range of 0.3–6 eV, depending on the bandgap of the material under investigation. The electrons and holes recombine either by radiative or by non-radiative processes. First electrons and holes relax to the band edges or the states in quantum structures by rapid non-radiative scattering processes. In the direct bandgap materials investigated in this thesis, the carrier pairs usually recombine radiatively via near band edge transitions. By measuring the spectrum of this luminescence, valuable information from the band structure and the carrier states in quantum structures can be extracted.

A schematic diagram of the PL measument setup used in this work is shown in figure 4.1. The sample is located in a closed cycle helium cryostat, in which the temperature can be varied between 9 K and room temperature. Most of the PL measurements in this thesis were made at 9 K. An argon ion laser (wavelengths 488 nm, 514 nm) or a frequency doubled Nd:YVO laser (532 nm) is used for excitation. The absorption coefficient of GaAs at these wavelengths is of the order of $10^5\,\mathrm{cm}^{-1}$ [46], which means that absorption and carrier generation occur mainly in the substrate below the quantum structure. The full width at half maximum of the

intensity distribution of the focused laser beam on the sample surface is typically 100 μm. If the areal density of QDs is of the order of 10^9 cm^{-2}, about 10^5 QDs are excited simultaneously.

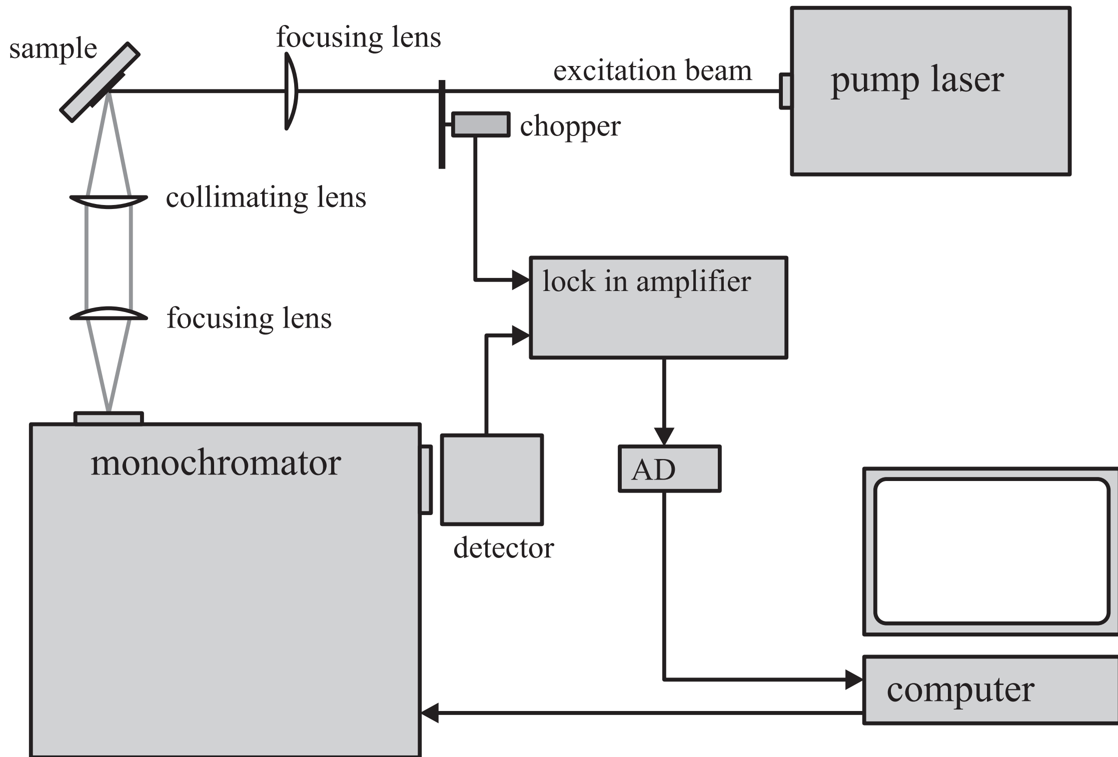

Figure 4.1: Schematic illustration of the continuous wave photoluminescence setup.

The luminescence is collected and focused with two lenses into a 0.5 m monochromator. A liquid nitrogen cooled germanium pin-diode is used as a detector. The standard lock in -technique is used to improve the signal-noise ratio of the detection. A computer with an AD converter is used to control the monochromator and collect the measurement data.

4.2 Time resolved photoluminescence

Time resolved photoluminescence (TRPL) is used to investigate the carrier dynamics. In a TRPL measurement the sample is excited with a very short and intense light pulse, and the luminescence is measured with the necessary temporal resolution. Luminescence intensities of the transitions depend on the corresponding recombination rates. Because the recombination rate depends on the carrier populations in the participating states, the carrier populations in different states can be calculated as a function of time. Therefore, also the transition processes between the participating states can be studied. In the QDs investigated in this work, the time constants of the phenomena related to the carrier dynamics are typically of the order of 1 ns. Immediately after the excitation pulse even more rapid processes have a major role, but due to the limitations of the detection system and the rate-equation model these processes were not studied in this thesis.

Figure 4.2 shows schematically the TRPL measurement system used in this work. The basic optics, beam focusing, sample cooling, luminescence collimating and monochromator were the same as in the continuous wave PL (CWPL) measurement system. The excitation pulse source was a mode locked titanium sapphire laser operating at the wavelength of 800 nm. The pulse length was approximately 150 fs, the pulse repetition rate was 76 MHz, and the energy of a single pulse was typically 10–100 pJ on the sample. If we assume the quantum efficiency to be 1.0, the number of electron hole pairs excited during one pulse is of the order of $10^{12}\,\mathrm{cm}^{-2}$. The absorption coefficient in GaAs is about $2 \cdot 10^{3}\,\mathrm{cm}^{-1}$ at the wavelength of 800 nm [46]. The carriers are generated mainly in the layer with the thickness of a few microns. This means that most of the carriers are generated in the substrate and they must diffuse into the QW and QDs before recombination.

The photon counting system uses a multichannel plate photomultiplier as a detector. Excitation laser pulses are detected by a silicon photodiode. The system measures

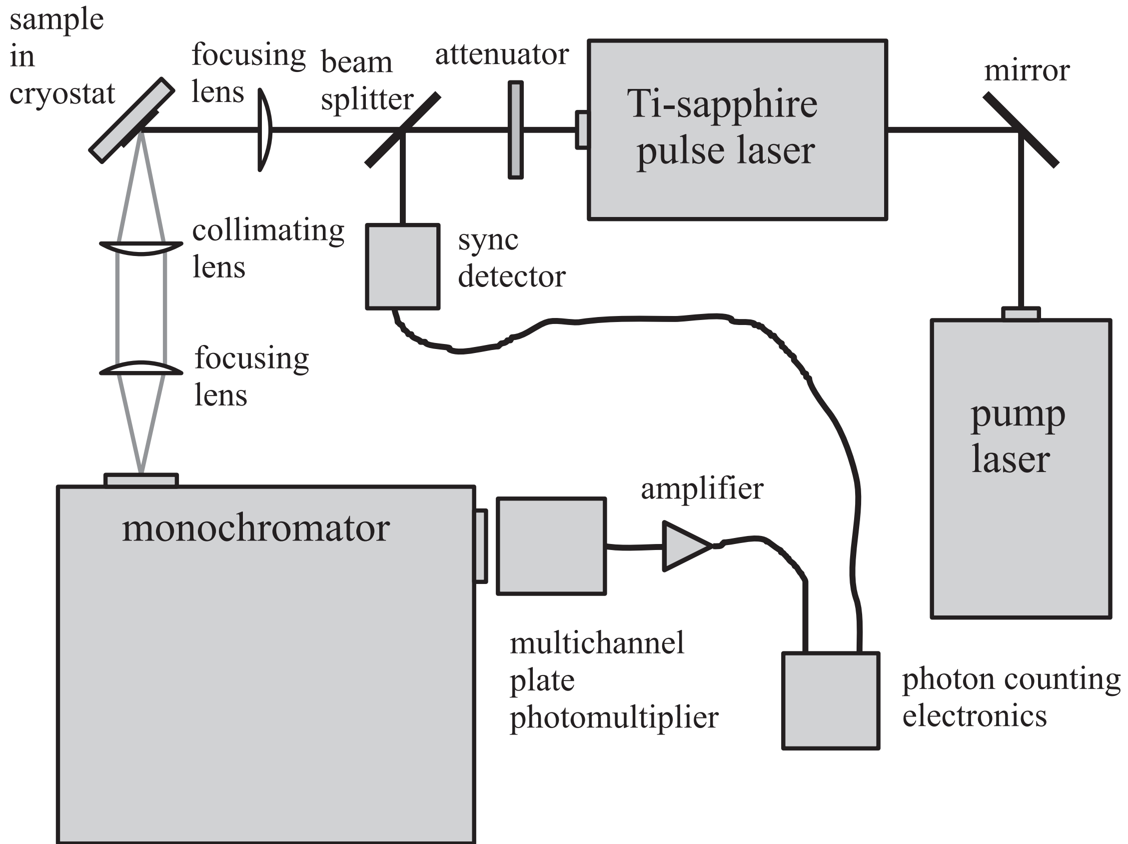

Figure 4.2: Schematic illustration of the time resolved photoluminescence setup.

the time between the detected PL photon and the next laser pulse. The system assumes, that only one photon is detected between two pulses, which determines the maximum intensity to about 10^6 photons per second. The temporal resolution of the photon counting system is about 30 ps. It is mainly determined by the photomultiplier tube.

4.3 Atomic force microscopy

Atomic force microscopy (AFM) was invented by Binnig *et al.* [47]. The AFM method is combining the principles of the scanning tunneling microscope and the

stylus profilometer. In AFM the topography of the sample surface is scanned by a sharp probe tip. The AFM technique can be used with conductive or nonconductive samples. The method is robust, because any special sample preparation is not needed and the measurement can be done in ambient air. The operating principle of the AFM is shown in figure 4.3. A sharp silicon nitride tip is attached to a cantilever, from which a laser beam is reflected to a segmented photodiode. When the tip is brought to a close vicinity of the sample surface, the electrostatic repulsion between the sample and the tip bends the cantilever, which moves the position of the laser beam on the photodetector. An electronic feedback loop and a piezoelectric actuator, which moves the sample in the vertical direction, are used to keep the distance between the tip and the surface constant. The feedback signal is used in determining the height of the features on the sample surface. The AFM system also has piezoelectric actuators to move the sample in the lateral directions. When the square shaped area is scanned row by row and the height data is collected by a computer, a three dimesional map of the surface sample can be formed.

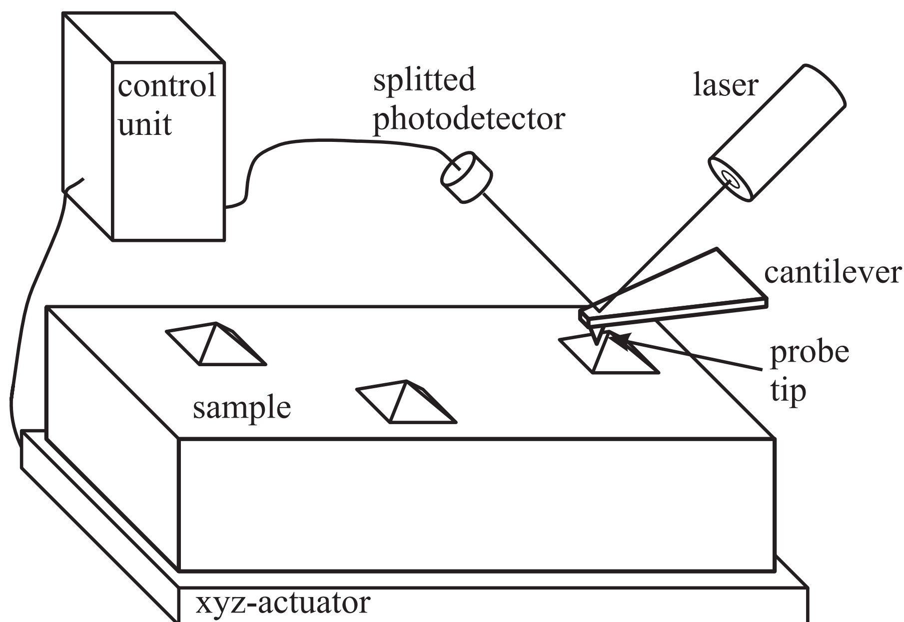

Figure 4.3: Schematic diagram of the AFM setup used in this thesis.

In this thesis, the atomic force micrographs were taken with a Nanoscope III E contact mode AFM. The maximum lateral scan area was $13 \times 13\ \mu\mathrm{m}^2$. The nominal radius of curvature of the silicon nitride tips used in this thesis was 10 nm. The measured height field is a convolution of the tip shape and the surface topography. However, in this work the effect of this convolution was neglected, because very accurate lateral sizes of the surface structures were not needed. Practically the errors in lateral dimensions are in the order of ten nanometers. The vertical resolution of the system is such that the system is capable to clearly resolve height variations of a single monolayer, about 0.2 nm.

5 SIQD results

In this chapter, the results of the SIQD studies are discussed. The optical properties of the GaInAsN SIQDs investigated in publication I are outlined in section 5.1. The optical properties of the novel GaInAsP/InP SIQDs, which has been studied in publication II, are discussed in section 5.2. Section 5.3 describes the effect of surface states in the carrier dynamics in GaInAsP/InP SIQDs, which were studied in publications III and IV. In publication V the rate equation model is improved by taking into account a gaussian excitation beam distribution. This study is discussed in section 5.4. Section 5.5 describes the investigation of electron states and the carrier dynamics in coupled SIQDs.

5.1 SIQDs with dilute nitrides

In recent years GaInNAs grown on GaAs has been studied intensively, because the possibility of lattice matching with the GaAs substrate makes GaInNAs potentially suitable for optical communications at the wavelengths of 1.3 and 1.55 μm. Applications of GaInNAs quantum wells, such as laser diodes having improved high-temperature performance [48], vertical cavity surface emitting lasers [49] and efficient multi-junction solar cells [50] have been reported. In publication I, GaInAsN SIQDs were fabricated and optically characterized. Samples with a 8 nm thick $Ga_{0.8}In_{0.2}N_yAs_{1-y}$ QW and a 5 nm thick GaAs barrier layer were grown at 530 °C on a 100 nm thick GaAs buffer layer. Thermal annealing at 650 °C was subsequently performed for 10 min to enhance the optical performance of the samples. After annealing 5 nm thick GaAs cap layer was grown on the barrier layer. Then an InP layer with a nominal thickness of 3 monolayers was fabricated. The material compositions are based on the growth data of Hakkarainen et al. [51].

Optical properties of the QDs have been studied with continuous wave and time resolved photoluminescence spectroscopy in publication I. The previously reported [52, 53] charge carrier localization in the nitrogen containing QWs has been observed. Adding nitrogen seems to result in concentration and thickness variations having a lateral feature size of less than 50 nm. The carrier localization is a consequence of these fluctuations.

The increase of N and In concentrations (y and $1-x$) is known to strongly reduce the band gap energy of $Ga_xIn_{1-x}N_yAs_{1-y}$. Low temperature (10 K) PL spectra of the samples with different nitrogen concentrations y are shown in figure 5.1 (a). The indium concentration was 0.2 in all the samples. PL peaks from the QW, the QD ground state (QD0) and the three excited QD states can be clearly seen in the spectrum of the nitrogen free sample. In the nitrogen containing samples the peaks are broader and typically only one excited QD state can be seen. Figure 5.1 (b) shows the low temperature PL peak energies of the QW and the QD0 states as a function of the nitrogen concentration. The QW peak shifts from 1.29 eV to 1.10 eV with increasing nitrogen concentration. The integrated PL intensity decreases to one tenth of the initial value when the nitrogen concentration of the QW increases from 0 % to 1.1 %. Recent studies suggest that interstitial nitrogen atoms form nonradiative recombination centers, which reduce the luminescence intensity [54].

Many of the observed results agree with the reported carrier localization into states located few tens of meV below the band edge of the QW [52, 53]. Figure 5.2 (a) shows the full width at half maximum (FWHM) of the QW and QD0 PL peaks as a function of the nitrogen concentration. Increasing the nitrogen concentration from 0 % to 1 % increases the FWHM of the QW peak from 9 meV to 25 meV. The observed effect may indicate that the lateral variation in the composition or thickness takes place in the scale of less than the diameter of the QDs, which is about 50 nm. These fluctuations can form local potential minima in the QW, which may lead to suggested carrier localization.

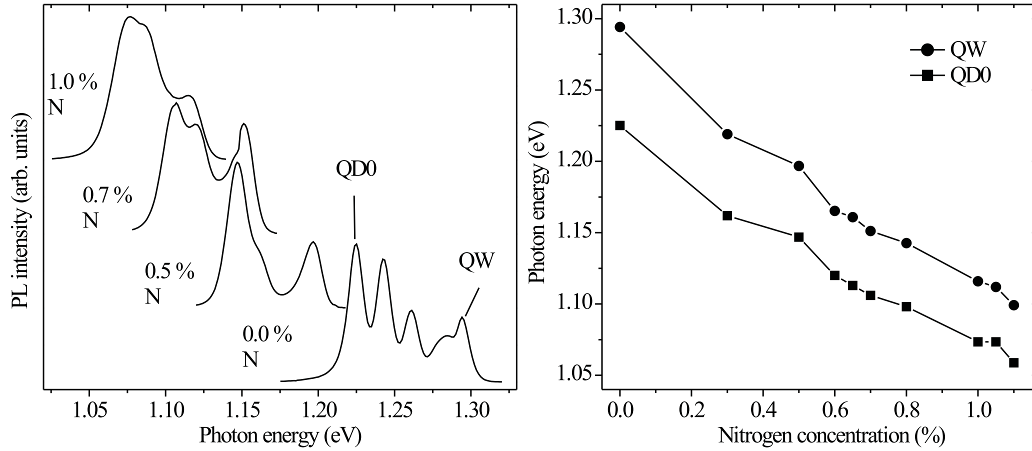

Figure 5.1: (a) Low temperature PL spectra of the samples with different nitrogen concentrations. QW and QD ground state (QD0) peaks have been marked. (b) Low temperature PL peak energies of the QW and the QD0 at different nitrogen concentrations.

Figure 5.2 (b) shows the energy separation between the QW and the QD ground state peaks as a function of the nitrogen concentration. The energy difference of the peaks decreases sharply from 69 meV of the nitrogen-free sample to 45 meV at about 0.6 % nitrogen concentration. The energy difference continues to decrease to about 40 meV, at the nitrogen concentration of about 1.1 %. Carrier trapping could explain also such a decrease in the energy difference. The gradual decrease of the energy separation at low nitrogen concentration suggests, that the depth of the localized states depends on the nitrogen concentration. Potential minima originated from the QW width, composition or strain fluctuations can have such a dependence, whereas the depth of the states originated from point defects in the crystal would be independent of the nitrogen concentration.

Figure 5.2 (c) shows the PL peak energies of the QW and QD ground states as a function of temperature for the samples with a nitrogen concentration of 0 %, 0.5 %

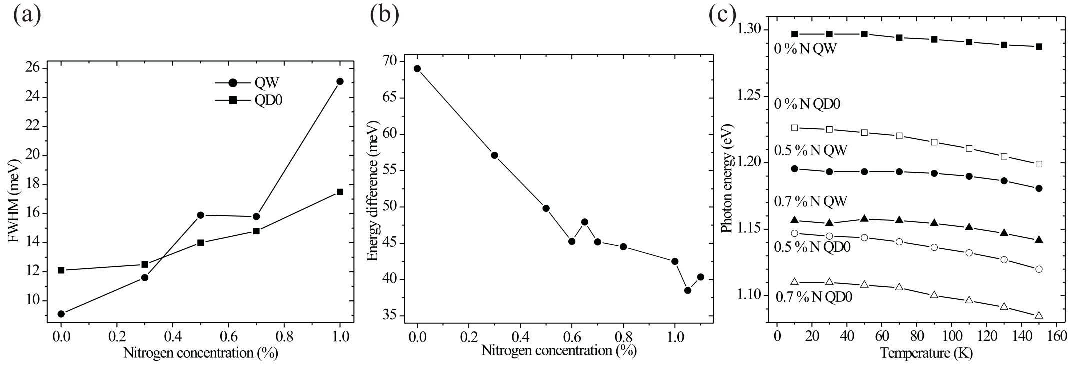

Figure 5.2: (a) Full width at half maximum (FWHM) of the low temperature QW and QD0 PL peaks at different nitrogen concentrations. (b) Low temperature PL peak energy difference between the QW and the QD0 peaks at different nitrogen concentrations. (c) PL peak energies of the QW and the QD0 transitions as a function of temperature for three samples with different nitrogen concentrations.

and 0.7 %. Especially in the 0.7 % sample a QW blueshift of about 3.5 meV can be seen between 30 and 50 K. Shirakata et al. have also observed such an effect in the as-grown $Ga_{0.65}In_{0.35}N_{0.01}As_{0.99}$ QW and explained it by thermal excitation of the localized carriers [55].

The low temperature time resolved PL intensities of the QW and the two lowest QD states for the nitrogen free sample and for the sample having a nitrogen concentration of 1.3 % are shown in figure 5.3. The luminescence decay time constant of the QW peak of the nitrogen-free sample and the sample containing nitrogen are about 0.4 ns and about 0.7 ns, respectively. The carrier localization is one possible explanation also for the slow decay in the latter case. When the carriers are trapped in the local QW states, they can not relax to the QD states before recombination. The decay time constant of the QD ground state peak is about 1.3 ns in both samples. The carrier localization does not affect the recombination rate of the QD states.

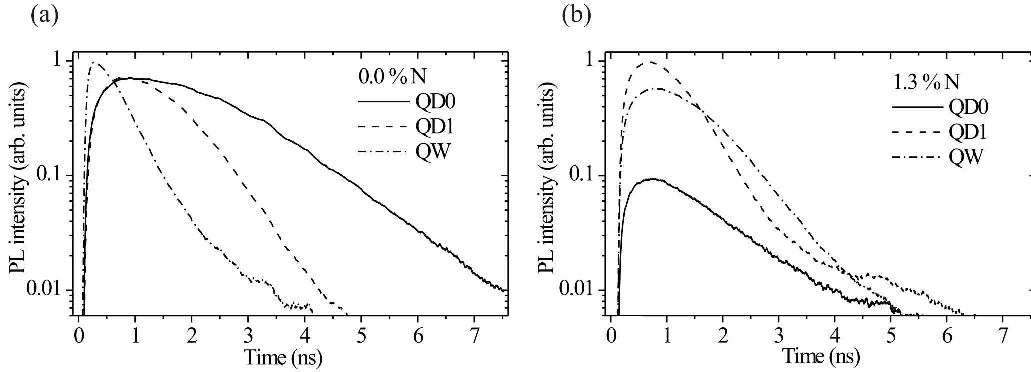

Figure 5.3: Low temperature time resolved PL intensities of the quantum well (QW), quantum dot first excited (QD1) and the quantum dot ground state (QD0) from samples with nitrogen concentration (a) 0 % and (b) 1.3 %.

5.2 Carrier dynamics in InGaAsP/InP SIQDs

SIQDs have been fabricated from many material systems, *e.g.*, by using InGaAs/GaAs [16], GaInNAs/GaAs [publication I], GaInP/AlGaInP [56], GaAs/AlGaAs [57], and SiGe/Si [58] QWs. In Publication II the effect of QW composition on the characteristics of the very recently introduced [59, 60] strain-induced InGaAs(P)/InP quantum dots are investigated. The distance of the QDs from the surface is also varied by adjusting the thickness of the QW and the InP capping layer. The details of the sample preparation by metal organic vapor phase epitaxy (MOVPE) are described in refs. 59 and 60. According to atomic force microscope (AFM) images, a typical island density, base diameter and height were $1 \cdot 10^9$ cm^{-2}, 100 nm, and 23 nm, respectively. The optical properties of the SIQDs were studied by low-temperature PL. PL measurements show that a wide low-temperature PL wavelength range from 1.3 to 1.7 mm is achieved. Numerical methods are used in the calculation of the QD energy levels which are shown to agree with the experimental data.

First, the PL emission wavelength of the InGaAs/InP SIQD was tuned by varying the QW composition. Structures with nearly lattice-matched or compressive InGaAs QWs showed typically good characteristics (the leftmost spectrum in figure 5.4). Using Gaussian fits, the separation between the QD peaks (*i.e.*, energy states) and the full width at half maximum (FWHM) of the QD peaks were determined to be about 16 and 13 meV, respectively. The almost equal level splitting between the QD states is a result of the nearly-parabolic confinement potential.

The Ga composition was further increased to blueshift the PL emission. The SIQDs with a slightly tensile QW seemed promising. However, with a higher Ga composition the PL peaks from the SIQD excited states became poorly resolved even though the morphology of the InAs stressor islands was similar to the samples with compressively strained QWs. This phenomenon has not been observed before, since in the previous SIQD systems the QW has always been compressively strained due to the constraints of the material system. Hence, the tensile strain ($\approx 1.0\%$) induced by the stressor island compensates the compressive strain in the QW. However, in the case of the InGaAs/InP QW, the induced strain may build up the tensile strain in the QW. In an unstrained QW the heavy-hole (HH) band is above the light-hole (LH) band due to QW confinement potential. On the other hand, the in-plane tensile strain moves the LH band to lower energy. This will lead to coupling of LH and HH bands which can explain why the QD peaks can not be resolved anymore. This strain related phenomenon will be investigated more closely in the future.

A viable means to overcome the strain related problem of the InGaAs QW is to utilize InGaAsP in order to fabricate a nearly lattice-matched QW. Using this approach, a wide low-temperature QD0 PL wavelength range from 1.3 to 1.7 mm was achieved as shown in figure 5.4 (a). Luminescence from the SIQD ground state was also observed at room temperature. It should be noted that the SIQD energy states compared to the QW are not significantly affected even as the bandgap of the QW is varied in a wide range ($\Delta E_{\mathrm{g}} \approx 0.25$ eV). Furthermore, it seems that even a wider

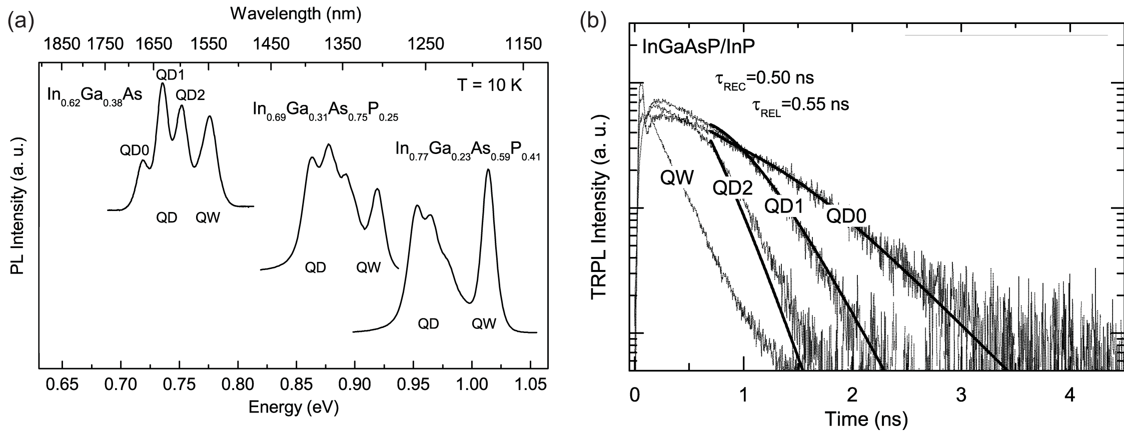

Figure 5.4: (a) Photoluminescence spectra showing the wavelength tunability of InGaAs(P)/InP SIQDs. (b) Time-resolved PL measurement of an InGaAsP/InP SIQD. Black lines represent the temporal behaviour calculated using the rate equation model.

wavelength range is feasible with this material system.

Additionally, low-temperature TRPL measurements were performed in order to gain insight into the carrier dynamics. SIQD intraband relaxation and interband radiative recombination rates were determined from the TRPL measurements using the rate equation model. The relaxation times were taken to be the same for intraband transitions and the carrier feeding from the QW to SIQD was ignored. Thus, the temporal behaviour only at low QW population was considered. In figure 5.4 (b), the calculated behaviour of the TRPL intensity (black lines) shows a good agreement with the measurements. The obtained relaxation and recombination time constants were $\tau_{\mathrm{rel}} \approx 0.55$ ns and $\tau_{\mathrm{rec}} \approx 0.50$ ns, respectively. The time constants for the other InGaAsP SIQD samples were about the same and are also close to the reported values for InGaAs/GaAs SIQDs ($\tau_{\mathrm{rel}} \approx 0.57$ ns and $\tau_{\mathrm{rec}} \approx 0.86$ ns [43]). However, the typical level separation is around 16 meV for InGaAs(P)/InP and 7–11 meV for InGaAs/GaAs [30]. This observation gives a clear indication that there is not any strong dependence of the relaxation time on the SIQD energy spacing.

The PL spectra were also measured from the nearly lattice matched InGaAs/InP SIQD samples with a varying InP cap thickness. The QD0 redshift from the QW increases by 17 meV while the capping layer thickness is decreased from 13 to 4 nm. The cap thickness has an effect on the redshift because the strain under the island decays as a function of depth, *i.e.*, the lateral confining potential becomes shallower. In addition to the cap thickness variation, the thickness of the QW was decreased from 13 to 7 nm in another series of samples. Besides the obvious increase of the QW transition energy (≈ 30 meV), the QW–QD0 redshift was also observed to increase. It should be noted that the cap thickness affects the redshift more efficiently than the QW thickness does. Computation using FEM was employed to calculate the strain induced by the stressor island, and, furthermore, the energy levels of QDs were calculated with the Schrödinger equation. The calculated values of the energy levels are in good agreement with the measured values. The QD0 redshift as a function of the distance from the surface to the QW center indicate that increasing the quantum well thickness affects the SIQD mainly by moving the center of the QW away from the surface, thus resulting in a shallower lateral confinement. This shows that the QW energy does not seem to affect the redshift or the level spacing, *i.e.*, the energy state structure of the QD significantly.

5.3 Surface effects in InGaAsP/InP SIQD structure

In the last decade, the carrier dynamics of GaInAs/GaAs SIQDs formed by InP stressors have been studied intensively. However, InP-based structures are needed for the operation at the 1.55 μm telecommunication wavelengths. Only a few works on carrier dynamics of GaInAs/InP near surface QWs have been published [61, 62]. In publications III and IV carrier dynamics in InGaAsP/InP SIQSs is investigated. In publication III the slightly compressively strained 10 nm thick $In_{0.77}Ga_{0.23}As_{0.59}P_{0.41}$ QWs were fabrigated on InP substrates. The thickness of the InP top barrier was varied from 4 nm to 13 nm. The self assembled InAs islands were grown on top of

the QW structure. As determined by AFM, the island density was approximately $2 \cdot 10^9 \mathrm{cm}^{-2}$ and the typical base diameter and the height of the islands were 110 nm and 22 nm, respectively.

The PL spectra in figure 5.5 (a) show that the PL intensities of the QD states decrease when the cap thickness is decreased. In publication III it was proposed that this is due to capture of carriers from the QD to the states in the InAs stressors or the wetting layer. Figure 5.5 (b) shows that the QD0 redshift, *i.e.*, the energy difference between the QW and the QD0 peaks, increases from 46 meV to 64 meV when the cap thickness is decreased from 13 nm to 4 nm. This is due to the fact that the strain, which induces the SIQD potential, decreases with the distance from the surface. In figure 5.5 (a), the intensity ratio of the QD peak to the QW peak decreases by nearly three orders of magnitude when the cap thickness is decreased from 13 to 4 nm. Thus, the carrier capture from the QD states to the surface seems to be a much more intense effect than the capture from the QW. The previous studies show that a thin InAs layer on InP causes surface depletion. However, electron accumulation in InAs islands suppresses the depletion under islands [63]. A similar result was suggested for the InAs/GaAs system [64]. It is also possible that the reduction of the vertical confinement due to the tensile strain induced by the stressor increases the surface capture rates under the stressor [59].

The standard rate equation model, as such, does not explain the carrier dynamics in our samples. To study the effect of the surface processes, a new equation to represent the population of electrons in the surface states was introduced. Transition rate terms from the QW and different QD states to the surface states were also added along with a surface recombination term. All the possible surface recombination transitions were included in one simple term. It was assumed that the capture rates from all the QD states (and the QW) to the surface state are proportional to the electron density in that QD state (and the QW) and to the density of empty surface states. The probability of the transition from the different QD states to the

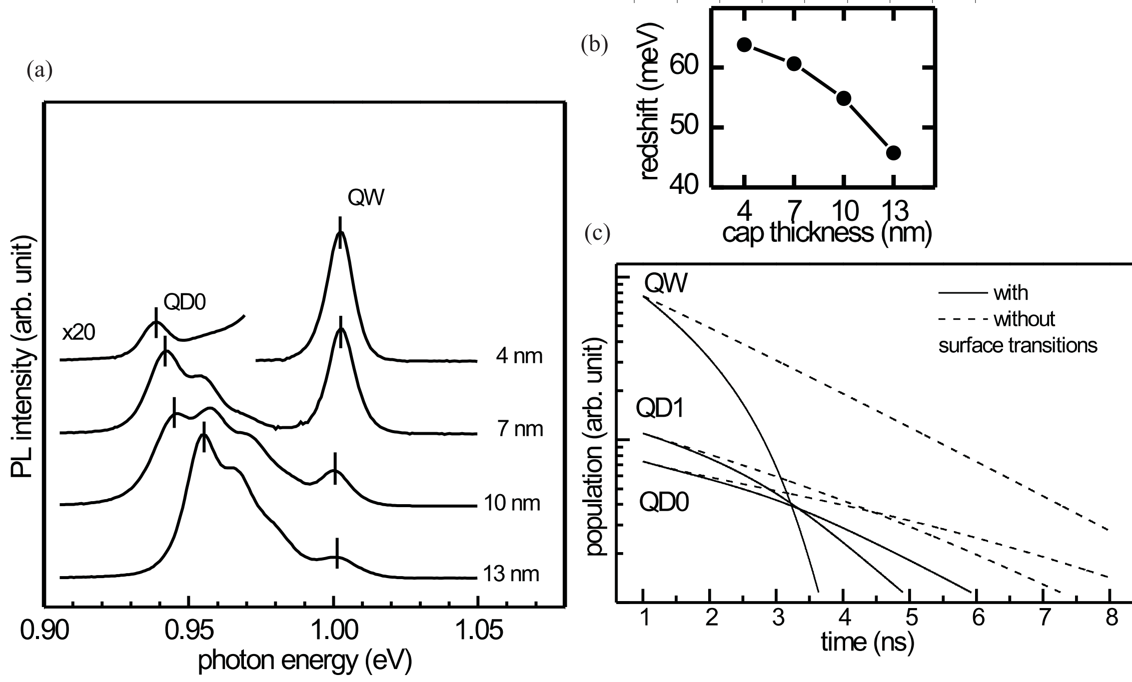

Figure 5.5: (a) PL spectra from the SIQD samples with cap thicknesses from 4 nm to 13 nm. (b) Redshift of the QD0 peak from the QW peak as a function of the cap thickness. (c) QD state and QW populations of a typical sample as a function of time calculated by the rate equation model with and without surface transitions.

surface states was assumed to be equal. The surface recombination rate was set to be linearly proportional to the electron density in the surface states. Also a new equation for the electron density in the QW was added to model. Probability of the electron capture from the QW to each QD level was assumed to be equal. All the above rates are also proportional to the electron density in the initial state and the density of available states in the final state. The modified rate equations can be written as

$$\frac{\mathrm{d}N_{\mathrm{QD},i}(t)}{\mathrm{d}t} = -\frac{N_{\mathrm{QD},i}(t)}{\tau_{\mathrm{rec,QD}}}+\frac{N_{\mathrm{QD},i+1}(t)}{\tau_{\mathrm{rel,QD}}}f_i(t)-\frac{N_{\mathrm{QD},i(t)}}{\tau_{\mathrm{rel,QD}}}f_{i-1}(t)+\frac{N_{\mathrm{QW}}(t)}{\tau_{cap}}f_i(t)-\frac{N_{\mathrm{QD},i}(t)}{\tau_{\mathrm{D},i\to\mathrm{s}}}f_s(t) \tag{5.1}$$

$$\frac{\mathrm{d}N_{\mathrm{QW}}(t)}{\mathrm{d}t} = -\frac{N_{\mathrm{QW}}(t)}{\tau_{\mathrm{rec,QW}}} - \frac{N_{\mathrm{QW}}(t)}{\tau_{\mathrm{cap}}} f_i(t) - \frac{N_{\mathrm{QW}}(t)}{\tau_{\mathrm{QW}\to\mathrm{s}}} f_s(t) \tag{5.2}$$

$$\frac{\mathrm{d}N_{\mathrm{s}}(t)}{\mathrm{d}t} = \frac{N_{\mathrm{QW}}(t)}{\tau_{\mathrm{QW}\to\mathrm{s}}} f_{\mathrm{s}}(t) + \sum_i \frac{N_{\mathrm{QD},i}(t)}{\tau_{\mathrm{QD}\to\mathrm{s}}} f_{\mathrm{s}}(t) - \frac{N_{\mathrm{s}}(t)}{\tau_{\mathrm{s}}} \tag{5.3}$$

The initial state was determined from the TRPL data. The saturation of the lowest QD states give the dependency between the electron density and the observed photon counts. We assume that recombination in the QW and the QD states is purely radiative. Due to the restrictions of the rate equation model discussed in chapter 3.3, the initial time in calculation is set to about 1 ns.

The dramatic effect of the surface processes is shown in figure 5.5 (c). The dashed curves are calculated electron populations using the parameters of a typical SIQD sample without the surface capture. The continuous curves are calculated with the same SIQD parameters, but taking into account the described surface processes. The surface processes lead to the observed subexponential slope of the transient curve.

The adjusted rate equation model was applied to analyze the temporal behaviour of the PL intensity of the two lowest QD levels and the QW peak. TRPL transients of the SIQD samples with a cap layer thicknesses of 7 nm, 10 nm and 13 nm are shown in figure 5.6 (a), (c) and (e), respectively. The corresponding populations calculated with rate equations are shown in figure 5.6 (b), (d) and (f). It can be observed that the thinner the cap layer is, the faster the PL intensity from the QD states and the QW decays. This trend can be explained by the increasing electron recombination via surface processes with the decreasing cap thickness. The values of time constants used in the rate-equation model are shown in figure 5.7.

In publication IV the capture rates from the QW to QDs was also calculated by an

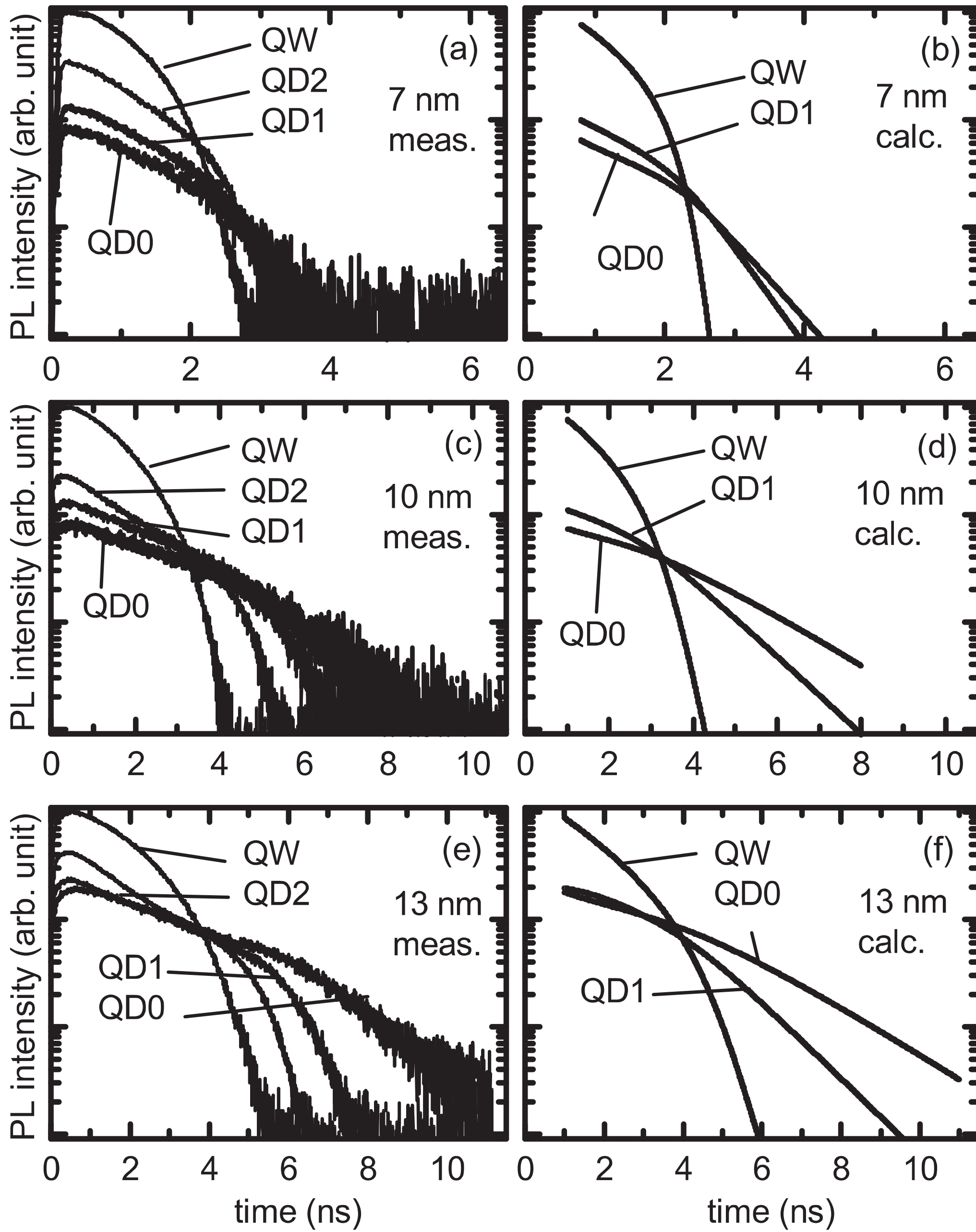

Figure 5.6: TRPL results from the samples with a cap layer thickness of (a) 7 nm, (c) 10 nm, and (e) 13 nm. The PL intensity curves from the QW, QD0, QD1, and QD2 states are shown. The corresponding rate equation calculations are shown in (b), (d), and (f).

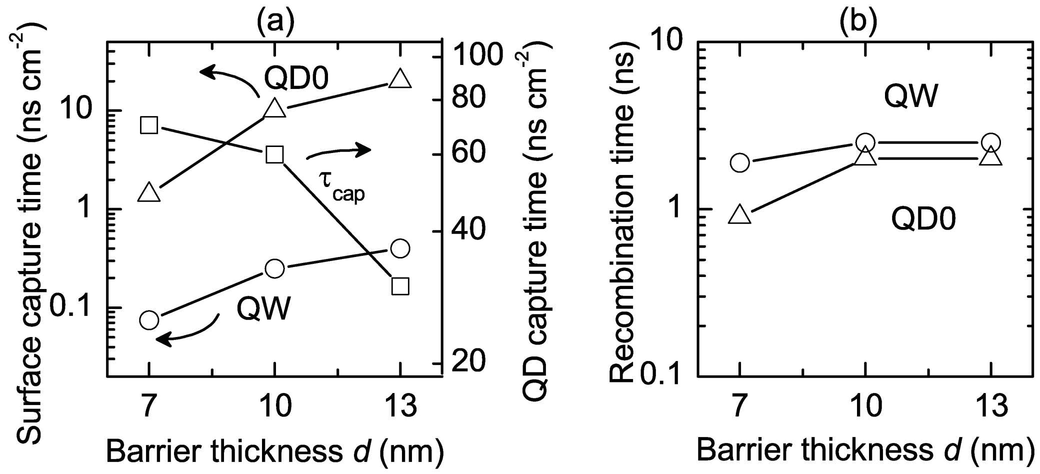

Figure 5.7: (a) Surface capture time constants for the QW and QD0 level and QD capture time constant (τ_{cap}) and (b) recombination time constants obtained for the QW and the QD0 level from the rate equation model.

other method. Lingk *et al.* [65] have shown that the capture rates can be calculated by equation

$$\eta_{\text{QD}}\tau_{\text{cap}} = \frac{I_{\text{QD}}}{I_{\text{QW}}}\tau^{-1}_{\text{rec,QW}}. \tag{5.4}$$

From figure 5.7 it can be seen that the radiative recombination times of the QW and QD transitions ($\tau_{\text{rec,QW}}$ and $\tau_{\text{rec,QD}}$) are virtually independent of d. In these conditions the capture rate can be written

$$\tau_{\text{cap}} = \frac{I_{\text{QD}}}{I_{\text{QW}}}\tau^{-1}_{\text{dec,QW}}, \tag{5.5}$$

where $\tau_{\text{dec,QW}}$ is the luminescence decay time constant of the QW. Results from this calculation agrees well with the results of the rate-equation model.

5.4 Effect of gaussian beam distribution in rate equation model

In publication V SIQDs were fabricated by growing a 4 nm thick InGaAs QW, a 5 nm thick GaAs barrier layer, and self assembled InP islands on the GaAs substrate. The samples were investigated by time resolved and continuous wave photoluminescence spectroscopy. Carrier dynamics was modeled with rate equations taking also into account the gaussian intensity distribution of the excitation beam.

It is well known that carrier dynamics modeled with rate equations explains with reasonable accuracy the TRPL curves measured from strain induced InGaAs/GaAs QDs [43]. In this work, the rate equation model was also used to calculate the CWPL intensities at various excitation conditions in addition to simulating TRPL curves. It has been shown that dynamics is determined by electrons only, because the relaxation of the holes is much more rapid than the relaxation of electrons and also because the samples fabricated with this MOVPE reactor have typically p-type background doping [43]. Therefore, the behaviour of holes can be omitted from the rate equation model.

The rate equation system used to simulate the electron populations in the QD levels and in the QW is written as

$$\frac{dN_i(t)}{dt} = -\frac{N_i}{\tau_{\mathrm{rec}}} + \frac{N_{i+1}(t)}{\tau_{\mathrm{rel},i+1}}\frac{D_i - N_i(t)}{D_i} - \frac{N_i(t)}{\tau_{\mathrm{rel},i}}\frac{D_{i-1} - N_{i-1}(t)}{D_{i-1}} + \frac{N_{\mathrm{QW}(t)}}{\tau_{\mathrm{QW}\rightarrow\mathrm{QD}}}\frac{D_i - N_i(t)}{D_i} \tag{5.6}$$

$$\frac{dN_{\mathrm{QW}}(t)}{dt} = G - \frac{N_{\mathrm{QW}}(t)}{\tau_{\mathrm{rec,QW}}} - \sum_{i=1}^{n}\frac{N_{\mathrm{QW}}(t)}{\tau_{\mathrm{QW}\rightarrow\mathrm{QD}}}\frac{D_i - N_i(t)}{D_i}, \tag{5.7}$$

where $N_i(t)$ is the electron density of the ith QD level normalized to D_i and $N_{\mathrm{QW}}(t)$

is the electron density per QD in the QW. The CWPL luminescence intensity of each transition is assumed to be propotional to the electron density in the corresponding electron level. G is generation of electrons and it is assumed to be proportional to the excitation intensity.

The recombination time constant in the QD states, τ_{rec}, is assumed to be equal for all the allowed QD transitions, whereas the recombination time constant of the electrons in the QW, $\tau_{\mathrm{rec,QW}}$, can be different from τ_{rec}. The time constant $\tau_{\mathrm{rel,i}}$ stands for relaxation from the ith QD level to the $(i-1)$th QD level. Relaxation between other combinations of QD states is assumed to be negligible [45]. The time constant can also be written as $\tau_{\mathrm{rel,i}} = (D_1/D_{i-1})\tau_{\mathrm{rel}}$ $(i \geq 2)$ due to the fact that the number of final states is proportional to D_{i-1}. It is assumed that the relaxation time does not depend on other parameters, so that τ_{rel} is constant.

The time constant of relaxation from the QW into the QD levels is marked with $\tau_{\mathrm{QW}\to\mathrm{QD}}$, which is used as a fitting parameter in the calculations. LO phonon scattering dominates relaxation from the QW to the QDs at carrier densities used in this study [40]. Therefore, $\tau_{\mathrm{QW}\to\mathrm{QD}}$ is assumed to be a constant independent of N_{QW}.

To determine the recombination and relaxation time constants for the rate equation model, the model calculations were fitted to the TRPL measurement data. Using the determined time constants, the CWPL peak intensities were simulated. As a first approximation, the generation was assumed to be laterally constant. The state filling of the QD states is clearly seen in figure 5.8 (a). However, the state filling effect in the measured PL intensity of the lower QD peaks is not as strong as can be seen in figure 5.8 (c). To improve the model, the beam intensity was modeled with a more realistic gaussian profile

$$I(r) = P\frac{\ln 2}{\pi r_{1/2}^2}\exp(-\ln 2(\frac{r}{r_{1/2}})^2), \tag{5.8}$$

where $r_{1/2}$ is the radius in which the intensity of the excitation beam is half of the maximum value and P is the excitation power. The beam area from the center ($r = 0$) to $r = 4r_{1/2}$ was divided into concentric rings and the PL intensities of these areas were then calculated with the rate equations. The overall PL intensities were calculated by summing the contribution from each ring weighted by the area of the ring. Calculated and measured PL intensities are shown in figure 5.8 (b) and (c), respectively. The calculation with the gaussian beam agrees well with the measured PL results.

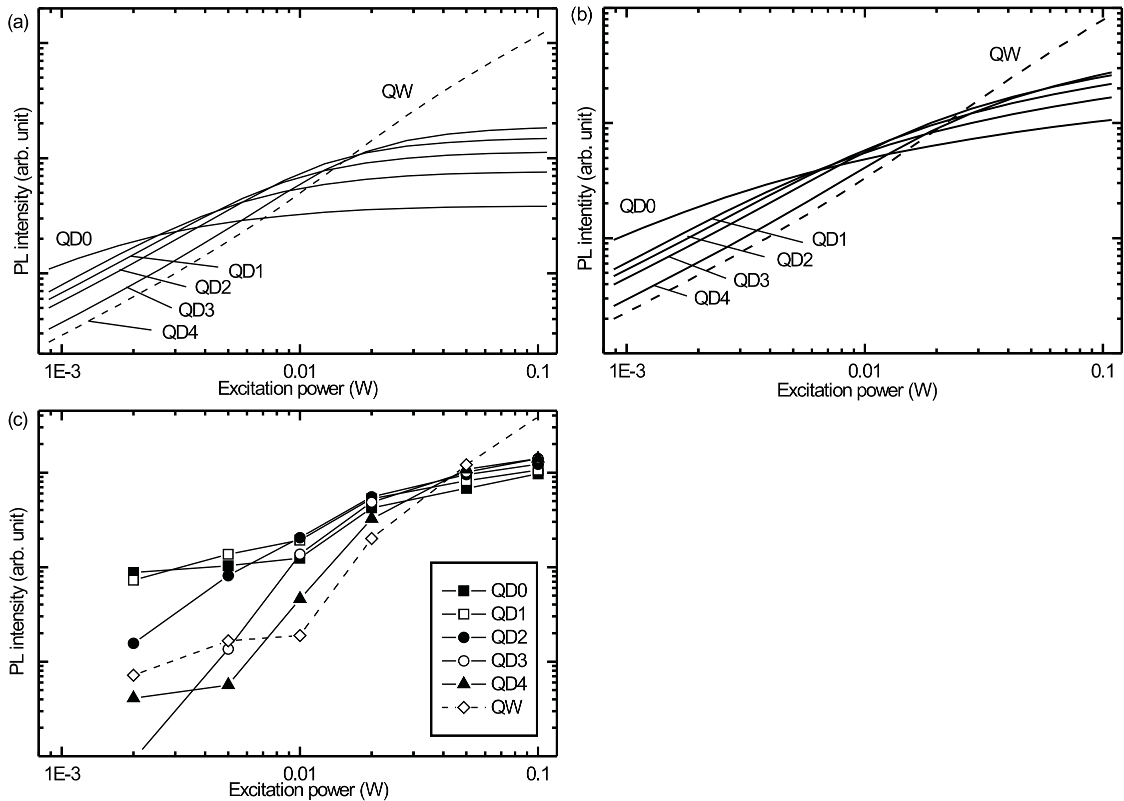

Figure 5.8: (a) CWPL intensities of the QW and QD states calculated by the rate-equation model assuming homogenous excitation beam profile. (b) Same as (a), but the gaussian excitation beam profile is taken into account. (c) Measured PL intensity of the QD and QW states as a function of excitation power.

In this publication we show that the rate-equation model can also be used to simulate CWPL data. We also include the gaussian profile of the excitation beam into

the model to get the saturation behaviour of QD transitions realistic. The extension of this approach would be to include the gaussian excitation beam profile into the TRPL simulation via rate equations. However, this seems to lead to an unsolvable problem of the initial populations. In CW excitation the assumption that all the carriers are generated in the QW or they are captured from bulk to the QW before recombination leads to a steady state which does not depend on the initial populations in the QD states. However, to model TRPL with rate equations and the gaussian beam distribution, the initial states of the QD populations as a function of location are needed. Unfortunately, they cannot be extracted from the TRPL data.

5.5 Modeling and PL study of coupled QDs

Over the past few years coupled quantum dots (QDs) have been fabricated by different methods. Several self-assembled InAs island layers separated by barriers have been grown [31, 32, 33, 34]. The formation of bonding and antibonding states in the double QDs have been reported [34, 66]. In recent years coupled QDs have attracted special interest in studies of quantum computation. Artificially controllable energy level structure and long decoherence time in comparison to bulk material make coupled QDs very useful for investigation of the entangled states [67, 68, 69]. In this so far unpublished work the coupled SIQDs was fabricated and their electronic states was calculated. Two 4 nm InGaAs QWs were grown on the GaAs substrate. The thickness of the GaAs barrier between the QWs was varied from 2 nm to 6 nm. A sample with one QW was fabricated for reference. On top of the upper QW a 5 nm GaAs barrier and self assembled InP islands were fabricated.

To study PL of double QDs, the electron states of the QDs were calculated. Details of the calculations are discussed in chapter 3.2. The results give the positions of the antisymmetric peaks compared to the symmetric peaks. The PL spectra of the samples and the calculated energies of the antisymmetric states are shown in figure

5.9. In the sample with a 2 nm thick barrier between the QWs, the energy of the lowest antisymmetric QD state is approximately the same as that of the QW ground state. Therefore, the state is not expected to be seen. In the 4 nm and the 6 nm samples, the calculated antisymmetric ground state peaks should be 51 meV and 47 meV higher than the QD0 peak, respectively. However, these states can not be resolved in the measured spectra.

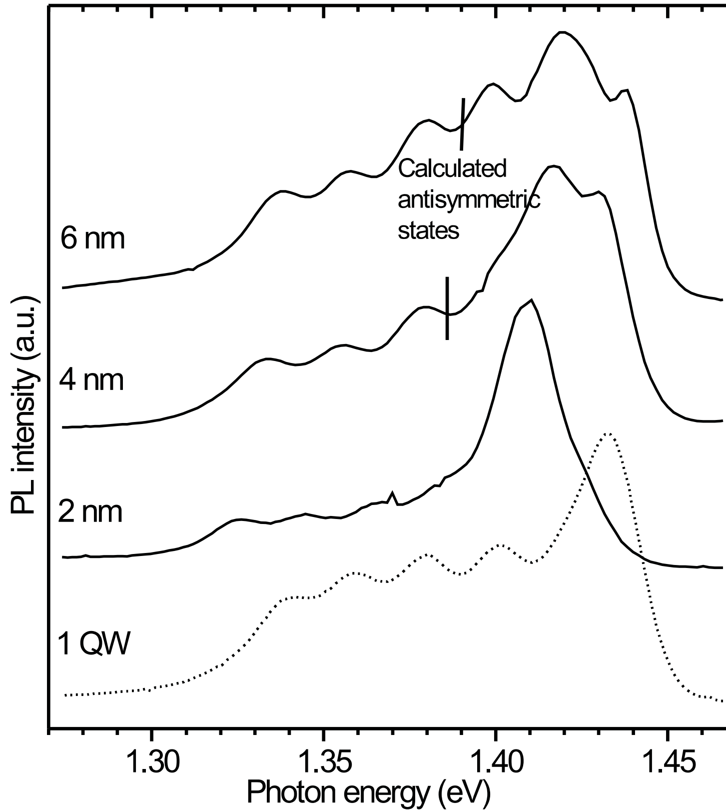

Figure 5.9: PL spectra of the samples with different barrier thicknesses between the QWs. The calculated positions of the lowest antisymmetric states are marked in the figure. There should not be any antisymmetric state below the QW state in the 2 nm sample.

Carrier dynamics in the double QD samples was very similar to carrier dynamics in the single QD reference sample. The recombination time constant increased from 1.45 ns to 1.60 ns, and the relaxation time constant increased from 0.55 ns to 0.6 ns, when the barrier thickness was varied from 2 nm to 6 nm. Recombination

and relaxation time constants of the single QD reference sample were 1.50 ns and 0.75 ns, respectively.

In this work the experimental detection of coupling could not be done. It is possible that due to the fabrication unideality of the samples the antisymmetric states is weak or so close to the PL peaks of the symmetric sates that they can not be resolved. Before publication this work should be continue by fabricating more samples with different barrier thicknesses and by varying depths of QWs independently to get better resonance between the states.

This study can be continued by fabricating more samples with different barrier thicknesses and by varying the composition of the QWs independently to line up the energy levels of the individual dots. This would reduce the width of at least the ground level peak and help to resolve the peak related to the antisymmetric state.

6 Other results

In this chapter, the results obtained from the other structures than SIQDs are outlined. Section 6.1 discusses GaNAs QDs on InP, which were studied in publication VI. In publication VII ultrathin gallium nitride passivation layers grown *in situ* on near-surface $In_xGa_{1-x}As$/GaAs QWs are reported. These results are outlined in section 6.2. Finally, section 6.3 discusses fabrication and measurements of InN films on sapphire, which were studied in publication VIII.

6.1 GaNAs QDs on InP

Stranski-Krastanow (S–K) growth of coherently strained islands has been under extensive study during the last two decades due to its potential to form high quality QDs. The research has been concentrated on compressively strained material systems, like InP on GaAs or InAs on InP. Also tensile three dimensional islands have been fabricated from, *e.g.*, PbSe on PbTe [70]. Growth of tensile systems does not necessarily produce coherent 3D islands, *e.g.*, holes on GaInAs layer grown on InP have been reported [71]. One problem with the tensile strained systems is that the tensile islands have typically a larger band gap than the host material. Therefore, these islands can not confine carriers and are not QDs. However, at least one tensile strained system, *i.e.*, $GaAs_{1-x}N$ on InP, theoretically has type-I band alignment at certain nitrogen compositions and can confine both electrons and holes. GaAs/InP heterojunction on an InP substrate has a type-II band alignment in which only holes are confined in GaAs. The conduction and valence band offset energies are approximately 172 and 550 meV, respectively [72]. Because the incorporation of nitrogen reduces the band gap of GaAsN by lowering the conduction band edge [73], it is expected that the transition to type-I interface would occur with a nitrogen composition of about $x = 0.013$. In publication VI, growth studies of the GaAsN on InP

system with a goal to achieve type-I quatum dot structures are presented.

The sample growth was carried out in a horizontal metalorganic vapor phase epitaxy (MOVPE) reactor. First, a 100 nm thick InP buffer layer was grown on a InP (100) substrate. After the growth of the buffer layer GaAsN was deposited at different temperatures varied in the range of 530–610 °C. The nitrogen composition is expected to be about 5.5 % with these growth parameters [74]. To study surface morphology by atomic force microscopy (AFM), part of the samples were left uncapped. In the rest of the samples the GaAsN layer was capped with an InP barrier layer for optical measurements. For reference, samples with thin layers (1–6 ML) of GaAs were grown on the InP buffer layer. In the samples, in which the GaAsN layer was grown below 610 °C, the islands were not observed. At 610 °C few islands were formed, but the material had otherwise accumulated to wire-like structures. Therefore, clear S–K growth mode could not be observed.

It has been found out that thermal annealing can be used to enhance island formation [75]. To optimize the nitrogen concentration, the samples were grown at 530 °C with varying GaAsN deposition thicknesses (3–6 ML). The samples were then in-situ annealed at 610 °C for 20 s. 3D islands were observed from the samples with the nominal GaAsN thickness of 4–5 ML.

Figure 6.1 shows low temperature PL spectra of buried GaAsN layers with different nominal thicknesses. The peaks in the energy range of 1.25–1.37 eV seem to originate from the GaAsN wetting layer (WL). The multiple peaks in the 3 ML sample correspond to different areas of the WL having 1 ML difference in the thickness. These 1 ML fluctuations are also observed in the AFM image of the uncovered layer. With the coverage of 4 ML and 5 ML the critical thickness is reached and the islands are formed. The luminescence peak centered at 1.05 eV originates from the islands. When the deposition thickness is increased to 6 ML the PL intensity clearly decreases. This can be explained by enhancement of the nonradiative recom-

bination due to dislocation formation associated with the relaxation of the islands. In addition, the wetting layer luminescence begins to dominate [76].

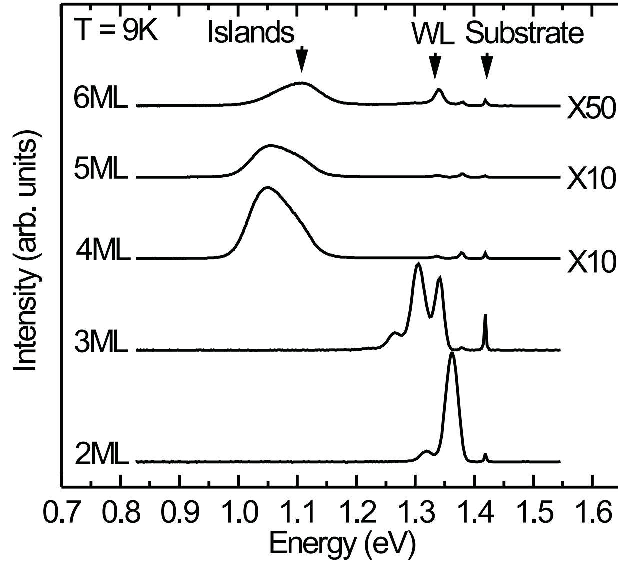

Figure 6.1: LT-PL spectra from the samples with various thicknesses of buried GaAsN layers on InP.

To examine the nature of the radiative transitions observed in the GaAsN samples, a GaAs reference sample was grown. The reference sample had a 6 ML thick layer of GaAs buried between InP layers. Figure 6.2 shows the PL spectra from this sample and a GaAsN sample grown with the DMHy/V ratio of 0.92. WL peaks at about 1.34 eV can be seen in both samples. In the GaAs reference sample the peak results from a type-II transition between the InP conduction band and the GaAs WL QW. In the GaAsN sample the wetting layer peak is approximately at the same wavelength. This can be explained by the fact that nitrogen modifies mainly the conduction band and does not have a noticeable effect on the valence band [73]. The band structure and the energy states of the GaAs/InP and GaNAs/InP quantum wells are shown in the inset of figure 6.2. Energy of the type-II WL peak is close to the band gap of InP, because the carrier states in a very narrow QW are very near the barrier potential. The several WL QW peaks are the result of the monolayer

thickness variations in the WL.

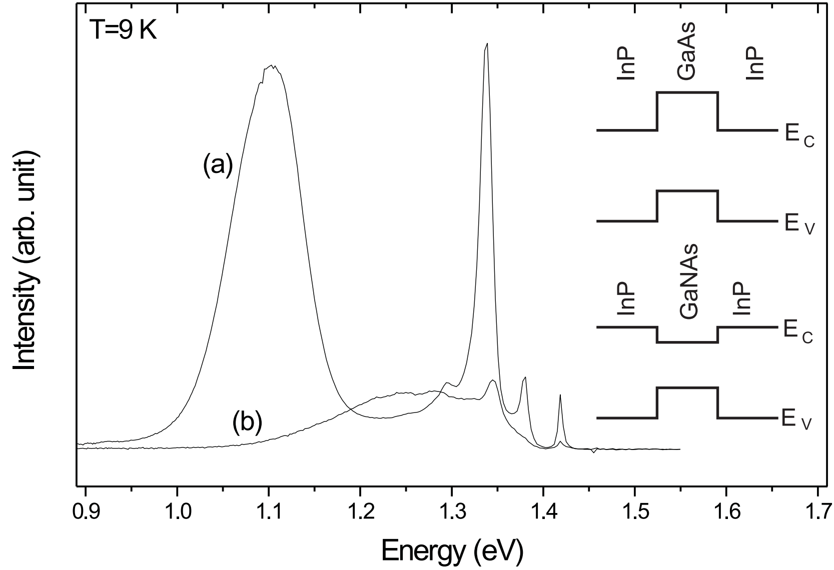

Figure 6.2: LT-PL spectra of the samples with a 6 ML thick buried layer of (a) GaAsN grown with the DMHy/V ratio of 0.92 and (b) GaAs. The energy band structures of the GaAs/InP and the GaNAs/InP QWs are shown in the inset.

In the PL spectrum of the GaAs sample a broad peak centered at 1.28 eV with a FWHM of 162 meV is observed. In the GaNAs sample a peak related to islands is centered at 1.1 eV and has a FWHM of 82 meV. Narrower and more intense peak in the GaNAs sample suggests that there may be a type-I transition in GaNAs QD, whereas type-II transition produces a weaker and broader peak in the GaAs sample. Also the wetting layer peak is strong in the GaNAs sample. This can be explained by the low confinement potential in the GaNAs conduction band of the GaNAs QDs. Thermal excitation throws electrons out from the shallow QD potential and they recombine in the WL QW.

The energetic positions of the peaks obtained from the GaAsN samples do not cor-

respond to the values calculated from a simple potential well model. The calculated values for the assumed nitrogen composition of x = 0.055 are somewhat lower. To investigate if any mixing of materials has occurred, an uncapped 6 ML thick GaAsN sample was investigated by X-ray photoelectron spectroscopy (XPS). XPS results indicates that mixing of materials in the interface of GaAsN and InP layers is possibly occurring. This cannot be asserted for sure because the thickness of the wetting layer is not known. However, mixing of materials does explain quite naturally the reason for the observed difference in the measured and calculated positions of the PL peaks.

6.2 GaN passivation of GaAs surface QW

The surface Fermi level pinning of GaAs, due to the high density of surface states, is a limiting factor in the performance of advanced electronic and optoelectronic devices, especially in low-dimensional structures. Thus, a variety of different passivation techniques have been studied to solve this problem. A variety of plasma nitridation methods [77, 78], Si-based insulators [79], and in situ grown InP passivation layers [80, 81] have been reported. In publication VII, the epitaxial *in situ* GaN passivation of GaAs is reported. Low temperature photoluminescence (PL) is used to study the effect of passivation on InGaAs/GaAs QWs. PL intensity enhancement of up to almost three orders of magnitude was measured from GaN-passivated near-surface quantum wells as compared to the unpassivated samples.

The near-surface InGaAs/GaAs quantum well samples were grown in a horizontal MOVPE reactor at atmospheric pressure. A typical near-surface QW sample consists of a 100 nm thick GaAs buffer layer, an $In_xGa_{1-x}As$ QW and a GaAs top barrier layer. The indium fractions (x) of the 6 and 4 nm thick quantum wells are 20 and 25%, respectively. The thickness of the GaAs cap is 5 nm. Two different surface passivation methods using DMHy were employed on the near-surface quan-

tum wells. In the first method, a nominally 1–3 ML thick GaN layer was grown at 550 °C. In the second method, after the growth of the top barrier GaAs, the TBAs flow was switched to DMHy at 600 °C to form a thin GaN layer via As-N exchange. After approximately 70 s of cooling, the DMHy flow was switched off at 400 °C. For reference, the same structures were grown without passivation. A deep QW sample with a 20 nm thick GaAs top barrier layer was used as a reference.

The PL spectra of the as-grown unpassivated, nitridated, and GaN-passivated 4 nm thick $In_{0.25}Ga_{0.75}As$/GaAs near-surface QWs with a top barrier thickness of 5 nm are shown in figure 6.3 (a). A deep QW structure with the top barrier thickness of 20 nm is shown as a reference. The PL intensity of the GaN-passivated sample is enhanced by a factor of 21 compared to the unpassivated QW. A small red shift of 2.8 meV can be seen in the PL spectrum of the GaN-passivated quantum well compared to the unpassivated structure. This behavior is probably caused by the formation of GaN_yAs_{1-y} on the GaAs-GaN interface due to As-N exchange. Thus, the QW barrier is presumably reduced because GaNAs has a lower band gap than GaAs. This is seen as a red shift of the PL peak. This assumption is supported by the fact that even a larger red shift (4.9 meV) is evident in the spectrum of $In_xGa_{1-x}As$ QW passivated with the nitridation method. It can be expected that in the nitridation process the As-N exchange is more pronounced and the GaN layer is thinner, effectively leading to even larger reduction of the QW barrier.

AFM studies show that small 2D islands can be seen on the GaAs atomic layer terraces on a deep QW and unpassivated samples. These are presumably GaAs islands. In GaN-passivated and nitridation passivated samples, no such small islands are seen. However, the surface morphologies are typical to 2D island growth with larger islands near the step edges. No clear difference can be observed between the epitaxial GaN layer and the nitridated GaAs surface. All in all, the passivation treatments do not seem to degrade the surface morphology of the samples.

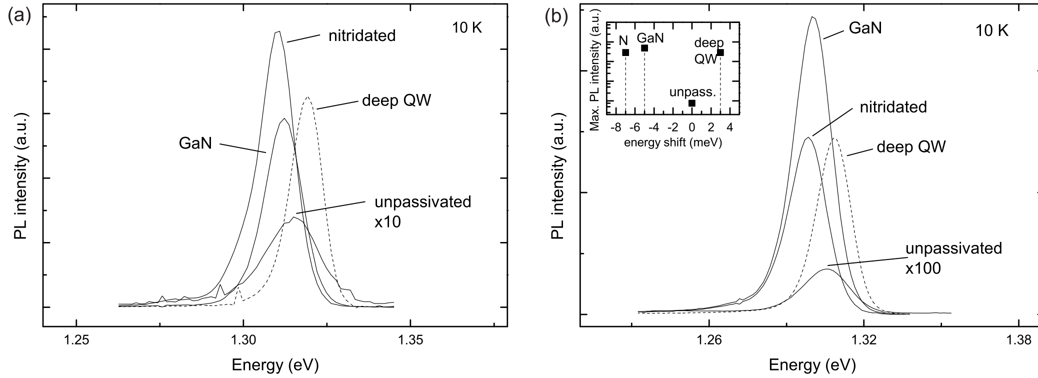

Figure 6.3: (a) PL spectra of the as-grown passivated 4 nm thick $In_{0.25}Ga_{0.75}As/GaAs$ near-surface QWs. The PL intensities of the passivated samples are enhanced and the peaks are slightly red shifted as compared to the unpassivated QW. (b) PL spectra of the same samples after storing about 5 months in ambient air. The intensity of the GaN passivated sample is nearly three orders of magnitude larger when compared to that of the unpassivated sample.

The effect of the thickness of the GaN passivation layer on the PL of the near-surface quantum wells was studied by varying the growth time of GaN. Small blue shifts of 1.3 and 3.9 meV are observed as the nominal thickness of GaN is increased from 1ML to 2 ML and 3 ML, respectively. This shows that a thicker GaN layer with the band gap larger than that of GaAs compensates the red shift seen in figure 6.3. This may be explained by the fact, that effect of the surface states is decreased when the distance from surface is increased.

PL measurements of 4 nm thick $In_{0.25}Ga_{0.75}As/GaAs$ near-surface QWs were carried out after storing the samples for about 5 months in ambient air. The spectra are shown in figure 6.3 (b). The PL intensity of the GaN-passivated sample is nearly 10^3 times larger compared to the unpassivated QW. The intensities of nitridated, GaN-passivated, and deep-QW structures are in the same order of magnitude. This implies that nitridation and GaN passivation have protected the samples against

degradation caused by oxidation.

6.3 Optical properties of InN

In publication VIII InN films were grown by MOVPE. The grown films are characterized with x-ray diffraction, AFM, PL, and Hall measurements. The InN films, grown on sapphire substrates, contain metallic indium and the film surface consist of hexagonal islands. Growth temperature has a strong effect on the island size, optical quality and electrical properties of the InN layer. The PL results suggest that the bandgap of InN is in the range of 0.7–0.9 eV.

Pure indium nitride is the least known of the III/N materials. The growth of high quality InN films has proven to be difficult. This is mainly because of the small growth temperature window. The growth temperature is limited from above by the desorption of nitrogen and thermal decomposition of the films [82]. From below the growth temperature is limited by low thermal decomposition rate of ammonia (NH_3) [83]. Also the formation of metallic indium is a well-known problem [84]. In publication the VIII first reported data on MOVPE growth of InN by vertical close coupled showerhead (CCS) reactor is reported. Epitaxial films of InN were grown on c-plane sapphire substrates by using TMIn and NH_3 as indium and nitrogen precursors, respectively. The technical details of growth process is presented in publication VIII. The thickness of the InN layer was varied between 400 and 1000 nm.

The growth rate of InN as a function of the TMIn supply at various temperatures shows a linear dependence on the TMIn flow in the temperature range from 500 °C to 650 °C. This indicates that the growth rate is limited by the amount of reactive indium, and not by the NH_3 decomposition rate as has previously been reported [85]. In the presence of sufficient nitrogen supply the growth temperature governs the island size, optical quality and electrical properties of the films. These observations

suggest that the cracking of NH_3 at temperatures around 600 °C is enhanced in the CCS reactor compared to the horizontal reactors.

AFM scans show that the film surface consists of 3D islands and that the island size increases with increasing growth temperature. When the growth takes place at mbox650 °C the islands have a clear hexagonal base shape, but with growth temperatures of 600 °C and 550 °C the exact shape is not so easy derermine. The root mean square (RMS) surface roughness drops from 64 to 13nm as the temperature is lowered from 650 to 550 °C.

A reflection from metallic indium is found in the x-ray diffraction curve. Metallic indium crystallizes in tetragonal lattice [86]. The amount of metallic indium was found to increase with increasing temperature and to be independent of the V/III ratio. Threshold temperature for the formation of metallic In was between 550 and 600 °C. These results indicate that the formation of metallic In is caused by the desorption of nitrogen at high temperatures, rather than by the shortage of reactive nitrogen during growth.

To evaluate the crystalline quality, full width at half maximum (FWHM) values of the XRD peaks were calculated from the ω–2θ and ω scans of the InN (0 0 2) reflection. These observations suggest that the films consist of domains with hexagonal single-phase crystal structure that are tilted with respect to each other. These domains can be seen as hexagonal islands on the sample surface. Stress caused by the large lattice mismatch between the substrate and film is relaxed by dislocation formation.

Many previous reports suggest that the bandgap of InN is about 2 eV [3, 87]. In our study, no emission was observed near this range. Figure 6.4 shows the PL spectra measured from the samples grown at 550, 600 and 650 °C. Luminescence in the range of 0.78 to 0.85 eV was observed from all the samples. This evidence

of the smaller band gap energy is congruent with the previous results obtained at room temperature [4]. Different crystallinity of the films [4] and bandgap widening due to oxygen contamination [88] are suggested as possible reasons for the observed bandgap values of around 2 eV.

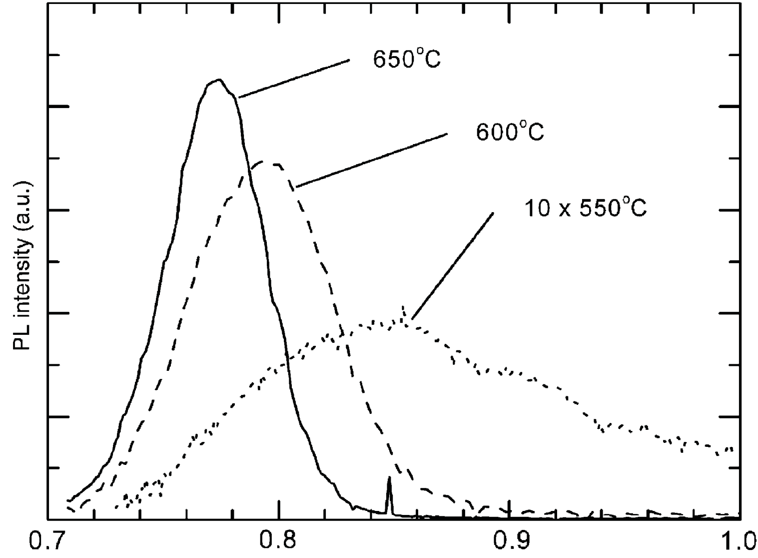

Figure 6.4: PL spectra of InN samples grown at different temperatures.

The PL peak intensity showed more than tenfold increase and the FWHM dropped from 133 to 37 meV as the growth temperature was increased from 550 to 650 °C. No change in the PL spectra was observed with different V/III ratios. The blue-shift of the PL peak energy with decreasing growth temperature is thought to result from the increase of the carrier concentration in the material grown at low temperature [89].

7 Summary

Semiconductor quantum structures have become an intensively studied topic in semiconductor technology. Due to the electron confinement and quantum mechanical effects they have special properties which can be utilized in electronic and optoelectronic components. In the last two decades the development of the manufacturing methods has enabled the fabricatrion of structures in nanometer and even atomary subnanometer scale with very high crystal quality.

In this thesis III–V semiconductors were characterized by photoluminescence spectroscopy and time resolved measurements. The main focus was in strain induced quantum dots (SIQDs). In the SIQD structure the quantum dots (QDs) are formed in the near surface quantum well layer by the tensile strain induced by nanometer scale stressors on top of the structure. This simple structure without the interface effects of the buried QDs provides an excellent method to investigate the basic properties of the QDs and the materials. However, the SIQD structure is difficult in the view of applications, because it is almost impossible to make electric contacts, mirrors or waveguide layers on top of the stressors without damaging the strain field.

Quartz optical fibres have an optimal performance at the wavelengths of 1.3 μm and 1.55 μm. In this thesis some materials which have a potential to function at these ranges have been investigated. The dilute nitrides are very interesting materials for this purpose. The optical properties and the carrier dynamics of the dilute InGaNAs/GaAs SIQDs were investigated. Also the GaNAs QWs and QDs on InP substrate were studied. GaNAs QDs on InP is the first tensile strained QD system made of III–V semiconductors.

GaInAsP/InP is a novel material system in the SIQD research. This material system can also be used in the telecommunication wavelength range. In this thesis carrier

dynamics in GaInAsP/InP SIQDs was investigated. It was observed that surface recombination has a major role in carrier dynamics. The rate-equation model was expanded to model surface transitions. The enhanced model agrees well with the time resolved photoluminescence data.

InGaAs/GaAs SIQDs were also studied. The gaussian excitation beam distribution was taken into account in the rate-equation model. The intensity vs. power relation of the continuous wave photoluminescense was modeled with good agreement to the measurements. The electronic states of the coupled InGaAs/GaAs SIQDs were calculated by the Schrödinger equation from the strain field calculated by the finite element method, but the calculated antisymmetric state was not detected experimentally.

In addition to the studies of the SIQDs, surface passivation of GaAs by thin epitaxial GaN layers was investigated. Optical measurements show that the GaN layer with the thickness of few monolayers can efficiently passivate the GaAs surface and also protect the GaAs surface against oxidation. Also InN films on sapphire substrates were investigated. It was observed that the bandgap of InN is in the currently established 0.6–0.9 eV region instead of 2 eV which was the common value in previous literature.

Based on the results presented, a number of further research topics can be suggested. The coupling of the valence bands in tensilely and compressively strained GaInPAs SIQDs can be calculated in more detail and the results can be compared to PL measurements of a larger set of samples. More accurate three dimensional modeling methods for coupled QDs together with improved fabrication methods can be further investigated. Single dot PL measurements, possibly in a magnetic field, would give valuable information about the electronic states in the single and coupled QDs by making it possible to resolve more transitions.

References

[1] Weyers M., Sato M. and Ando H. Japan. J. Appl. Phys. **32**, L853 (1992).

[2] M. Kondow, K. Uomi, A. Niwa, T. Kitatani, S. Watahiki and Y. Yazawa, Jpn. J. Appl. Phys. **35**, 1273 (1996).

[3] T. L. Tansley and C. P. Foley, J. Appl. Phys. **59**, 3241 (1986).

[4] T. Matsuoka, H. Okamoto, M. Nakao, H. Harima, E. Kurimoto, Appl. Phys. Lett. **81**, 1246 (2002).

[5] V.W.L. Chin, T.L. Tansley, T. Osotchan, J. Appl. Phys. **75**, 7365 (1994).

[6] G. W. Bryant, Phys Rev. B **37**, 8763 (1988).

[7] J. A. Venables, Surface Science **299/300**, 798 (1994).

[8] Z. Huang, Y. Wu, H. Fang, N. Deng, T. Ren, and J. Zhu, Nanotechnology **17**, 1476 (2006).

[9] F. C. Frank and J. H. van der Merwe, Proc. Roy. Soc. London **A198**, 216 (1949).

[10] M. Volmer and A. Weber, Z. Physik. Chem. **119**, 277 (1926).

[11] I. N. Stranski and L. Krastanow, Sitz. Ber. Akad. Wiss., Math. naturwiss. Kl. Abt. IIb **146**, 797 (1938).

[12] D. J. Eaglesham and M. Cerullo, Phys. Rev. Lett. **64**, 1943 (1990).

[13] S. Guha, A. Madhukar, and K. C. Rajkumar, Appl. Phys. Lett **57**, 2110 (1990).

[14] T. R. Ramachandran, R. Heitz, P. Chen, and A. Madhukar, Appl. Phys. Lett. **70**, 640 (1997).

[15] R. Nötzel, J. Temmyo, and T. Tamamura, Nature **369**, 131 (1994).

[16] M. Sopanen, H. Lipsanen, and J. Ahopelto, Appl. Phys. Lett. **66**, 2364 (1995).

[17] A. Ponchet, A. L. Corre, H. L'Haridon, B. Lambert, and S. Salaun, Appl. Phys. Lett. **67**, 656 (1995).

[18] F. Hatami, N. N. Ledentsov, M. Grundmann, J. Bohrer, F. Heinrichsdorff, M. Beer, D. Bimberg, S. S. Ruvimov, P. Werner, U. Gosele, et al., Appl. Phys. Lett. **(**67), 656 (1995).

[19] K. Kash, J. M. Worlock, M. D. Sturge, P. Grabbe, J. P. Harrison, A. Scherer, adn P. S. D. Lin, Appl. Phys. Lett **53**, 782 (1988).

[20] Z. Xu, M. Wassermeier, Y. J. Li, and P. M. Petroff, Appl. Phys. Lett. **60**, 586 (1990).

[21] K. Kash, J. M. Worlock, D. D. Mahoney, A. S. Gozdz, B. P. Van der Gaag, J. P. Harbison, P. S. D. Lin, and L. T. Florez, Surface Science **228**, 415 (1990).

[22] J. A. Yater, A. S. Plaut, K. Kash, P. S. D. Lin, L. T. Florez, J. P. Harbison, S. R. Das, and L. Lebrun, J. Vac. Sci. Technol. B **13**, 2284 (1995).

[23] ANSYS is registered trademark of ANSYS, Inc.

[24] I. Vurgaftman, J. R. Meyer, L. R. Ram-Mohan, Journal of Applied Physics **89**, 5815 (2001).

[25] D. Gershoni et al., Phys. Rev. B, **40**, 10017 (1989).

[26] G. E. Bikus and G. L. Bir, Fiz. Tverd. Tela **1**, 1642 (1959) [Sov. Phys. Solid State **1**, 136 (1959)].

[27] T. B. Bahder, Phys. Rev. B **41**, 11992 (1990).

[28] Mats Braskén, Doctoral thesis, Åbo Akademi 1999.

[29] J. Tulkki, A. Heinämäki, Phys. Rev. B, **52**, 8239 (1995).

[30] H. Lipsanen, M. Sopanen and J. Ahopelto, Phys. Rev. B **51**, 13868 (1995).

[31] Q. Xie, A. Madhukar, P. Chen, and N. P. Kobayashi, Phys. Rev. Lett. **75**, 2542 (1995).

[32] G. S. Solomon, J. A. Trezza, A. F. Marshall, and J. S. Harris, Jr., Phys. Rev. Lett **76**, 952 (1996).

[33] M. Sopanen, H. Lipsanen, J. Tulkki, and J. Ahopelto, Physica E **2**, 19 (1998).

[34] H.-W. Ren, S. V. Nair, J.-S. Lee, S- Sugou, and Y. Masumoto, J. Electronic Mat. **29**, 520 (2000).

[35] R. Virkkala, K. Maijala and J. Tulkki, Phys. Rev. B **62**, 6932 (2000).

[36] R. Rinaldi, S. Antonaci, M. De Vittorio, R. Cingolani, U. Hohenester, E. Molinari, H. Lipsanen, and J. Tulkki, Phys. Rev. B **62**, 1592 (2000).

[37] Y. Wada and K. Wada, Appl. Phys. Lett. **63**, 379 (1993).

[38] U. Bockelmann, T. Egeler, Phys. Rev. B **46**, 15574 (1992).

[39] J. H. H. Sandmann, S. Grosse, G. von Plessen, J. Feldmann, G. Hayes, R. Phillips, H. Lipsanen, M. Sopanen, and J. Ahopelto, Phys. Stat. Sol. **164**, 421 (1997).

[40] M. Braskén, M. Lindberg and J. Tulkki, Phys. Stat. Sol. 164, 427 (1997).

[41] M. Braskén, M. Lindberg, M. Sopanen, H. Lipsanen, J. Tulkki, Phys. Rev. B **58**, 15993 (1998).

[42] T. F. Boggess, L. Zhang, D. G. Deppe, D. L. Huffaker, and C. Cao, Appl. Phys. Lett. **78**, 276 (2001).

[43] S. Grosse, J. H. H. Sandmann, G. von Plessen, J. Feldmann, H. Lipsanen, M. Sopanen, and J. Ahopelto, Phys. Rev. B **55**, 4473 (1997).

[44] M. Grundmann and D. Bimberg, Phys. Rev. B **55**, 9740 (1997).

[45] M. Grundmann, R. Heitz, D. Bimberg, J.H.H. Sandmann, and J. Feldmann, Phys. Stat. Sol. (b) **203**, 121 (1997).

[46] Jasprit Singh, Semiconductor optoelectronics, McGraw-Hill Inc., 1995.

[47] G. Binning, C. F. Quate, and C. Gerbe, Phys. Rev. Lett. **56**, 930 (1986).

[48] Kitatani T, Nakahara K.,Kondow M., Uomi K., Tanaka T., Japan. J. Appl. Phys. **39**, L86–87 (2000).

[49] Ellmers C., Höhnsdorf F., Koch J., Agert C., Leu S., Karaiskaj D., Hoffmann M., Stolz W., Rühle W., Appl. Phys. Lett. **74**, 2271–2273 (1999).

[50] Kurtz S., Allermann A.,Jones E.,Gee J., Banas J.,Hammons B., Appl. Phys. Lett. **74**, 729–731 (1999).

[51] Hakkarainen T., Toivonen J., Sopanen M., Lipsanen H., J. Cryst. Growth **234**, 631–636 (2002).

[52] Pinault M.-A., Tournié E., Appl. Phys. Lett. **78**, 1562–1564 (2001).

[53] Grenouillet L., Bru-Chevallier C., Guillot G., Gilet P., Duvault P., Vannuffel C., Million A., Chenevas-Paule A., Appl. Phys. Lett. **76**, 2241–2243 (2000).

[54] Spruyette S.,Coldren C.,Harris J.,Wampler W.,Krispin P., Ploog K. Larson M., J. Appl. Phys. **89**, 4401–4406 (2001).

[55] Shirakata S.,Kondow M.,Kitanani T., Appl. Phys. Lett. **80**, 2087–2089 (2002).

[56] Sopanen M., Taskinen M., Lipsanen H., and Ahopelto J., Appl. Phys. Lett. **69**, 3393 (1996).

[57] Wang T. and Forchel A., Appl. Phys. Lett. **73**, 1847 (1998).

[58] Kim E. S., Usami N., and Shiraki Y, Appl. Phys. Lett. **70**, 295 (1997).

[59] J. Sormunen, J. Riikonen, M. Mattila, M. Sopanen and H. Lipsanen, Nanotechnology **16**, 1630–1635 (2005).

[60] J. Riikonen, J. Sormunen, M. Mattila, M. Sopanen, and H. Lipsanen, Jpn. J. Appl. Phys. **44**, L518 (2005).

[61] E. Yablanovitch, R. Bhat, C.E. Zah, T.J. Gmitter, and M.A. Koza, Appl. Phys. Lett. **60**, 371 (1991).

[62] C. Symonds, J. Mangeney, G. Saint-Girons, I. Sagnes, Appl. Phys. Lett. **87**, 12107 (2005).

[63] K. Vicaro, M. Cotta, H. Gutierrez and J. R. R. Bortoleto, Nanotechnology **14**, 509 (2003).

[64] T. Takahashi, M. Yoshita, I. Kamiya, H. Sakaki, Applied Physics A, **66**, S1055 (1998).

[65] Lingk C. et al, Phys. Rev. B **62**, 13588 (2000).

[66] G. Schedelbeck, W. Wegscheider, Science **278**, 1792 (1997).

[67] G. Chen, N. Bonadeo, D. Steel, D. Gammon, D. Katzer, D. Park, L. Sham, Science **289**, 1906 (2000).

[68] L. Quiroga, N. F. Johnson, Phys. Rev. Lett. **83**, 2270 (1999).

[69] Z. Kis, E. Paspalakis, J. Appl. Phys. **96**, 3435 (2004).

[70] M. Pinczolits, G. Springholz, and G. Bauer, Appl. Phys. Lett. **73**, 250 (1998).

[71] P. Krapf, Y. Robach, M. Gendry, and L. Porte, Phys Rev. B **55**, R10229 (1997).

[72] D. Gershoni, H. Temkin, J. M. Vandenberg, S. N. G. Chu, R. A. Hamm, M. B. Panish, Phys. Rev. Lett. **60**, 448 (1988).

[73] W. Shan, W. Walukiewicz, J.W. Ager III, E. E. Haller, J. F. Geisz, D. J. Friedman, J. M. Olson, S. R. Kurtz, J. Appl. Phys. **86**, 2349 (1999).

[74] J. Toivonen, T. Hakkarainen, M. Sopanen, H. Lipsanen, J. Cryst. Growth **221**, 456 (2000).

[75] J. F. Carlin, R. Houdré, A. Rudra, M. Ilegems, Appl. Phys. Lett. **59**, 3018 (1991).

[76] Hanxuan Li, T. Daniels-Race, Zhanguo Wang, Appl. Phys. Lett. **74**, 1388 (1999).

[77] M. Losurdo, P. Capezzuto, G. Bruno, Appl. Phys. Lett. **81**, 16–18 (2002).

[78] S. Anantathanasarn, S. Ootomo, T. Hashizume, H. Hasegawa, Appl. Surf. Sci. **159/160**, 456–461 (2000).

[79] S. Anantathanasarn, H. Hasegawa, Appl. Surf. Sci. **190**, 343–347 (2002).

[80] Y. Wada, K. Wada, J. Vac. Sci. Technol. B **12**, 3084 (1994).

[81] H. Lipsanen, M. Sopanen, M. Taskinen, J. Tulkki, J. Ahopelto, Appl. Phys. Lett. **68**, 2216–2218 (1996).

[82] Q. Guo, O. Kato, A. Yoshida, J. Appl. Phys. **73**, 7969 (1993).

[83] M. Mesrine, N. Grandjean, J. Massies, Appl. Phys. Lett. **72**, 350 (1998).

[84] A.G. Bhuiyan, A. Yamamoto, A. Hashimoto, Y. Ito, J. Crystal Growth **236**, 59 (2002).

[85] A. Yamamoto, M. Adachi, A. Hashimoto, J. Crystal Growth **230**, 351 (2001).

[86] A. Krost, J. Bläsing, H. Protzmann, M. Lünenbürger, M. Heuken, Appl. Phys. Lett. **76**, 1395 (2000).

[87] K. Osamura, S. Naka, and Y. Murakami, J. Appl. Phys. **46**, 3432 (1975).

[88] A. G. Bhuyian, K. Sugita, K. Kasashima, A. Hashimoto, A. Yamamoto, V. Y. Davydov, Appl. Phys. Lett. **83**, 4788 (2003).

[89] K. Sugita, H. Takatsuka, A. Hashimoto, A. Yamamoto, Phys. Stat. Sol. B **240**, 421 (2003).

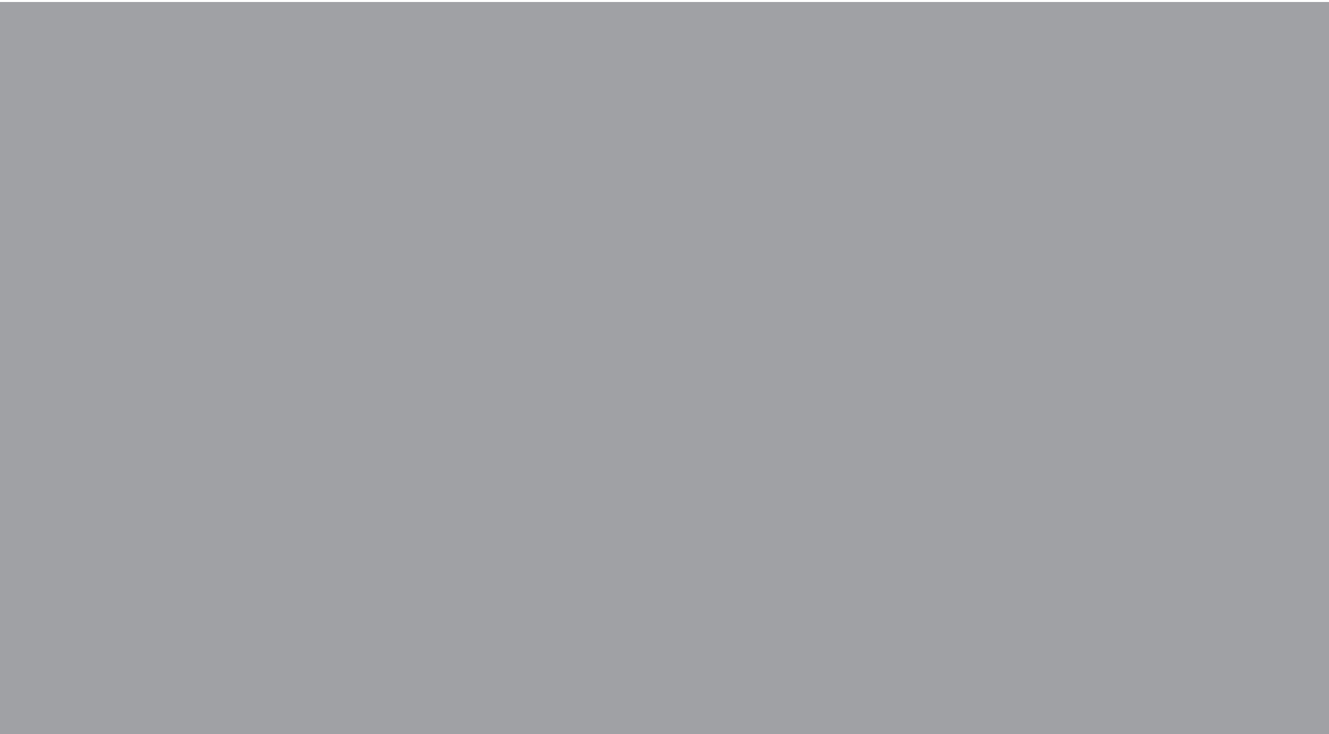

ISBN 978-951-22-9413-8
ISBN 978-951-22-9414-5 (PDF)
ISSN 1795-2239
ISSN 1795-4584 (PDF)